DRAFT

RFP-4074/13470/36331/81-0
UC-60

SMALL WIND ENERGY CONVERSION SYSTEMS (SWECS) ROTOR PERFORMANCE MODEL COMPARISON STUDY

Final Report

B. Hibbs and R.L. Radkey

AEROVIRONMENT, INC.
145 Vista Avenue
Pasadena, California 91107

November 1981

Prepared For
Rockwell International Corporation
Energy Systems Group
Rocky Flats Plant
Wind Systems Program
P.O. Box 464
Golden, CO 80401

Subcontract No. PFN-13470W

As A Part of The
U.S. DEPARTMENT OF ENERGY
DIVISION OF DISTRIBUTED SOLAR TECHNOLOGY
FEDERAL WIND ENERGY PROGRAM

Contract No. DE-AC04-76DPO3533

RFP-4074/13470/36331/81-0
UC-60

SMALL WIND ENERGY CONVERSION SYSTEMS (SWECS) ROTOR PERFORMANCE MODEL COMPARISON STUDY

Final Report

B. Hibbs and R.L. Radkey

AEROVIRONMENT, INC.
145 Vista Avenue
Pasadena, California 91107

November 1981

Prepared For
Rockwell International Corporation
Energy Systems Group
Rocky Flats Plant
Wind Systems Program
P.O. Box 464
Golden, CO 80401

Subcontract No. PFN-13470W

As A Part of The
U.S. DEPARTMENT OF ENERGY
DIVISION OF DISTRIBUTED SOLAR TECHNOLOGY
FEDERAL WIND ENERGY PROGRAM

Contract No. DE-AC04-76DPO3533

DISCLAIMER

PATENT STATUS

TECHNICAL STATUS

ABSTRACT

Recent interest in wind energy has increased the demand for accurate methods of wind turbine analysis. The purpose of this study was to make improvements to an existing AeroVironment wind turbine analysis computer code, PROP, developed by Wilson and Lissaman.

This involved analyzing two existing rotors, comparing the analytical results with experimental data, and making adjustments to the code, as required by comparing theory and experiment. Modifications to the code included addition of windmill brake state and wind shear effects, and refining treatment of blade airfoil characteristics.

The existing rotors analyzed with the modified code were the Enertech 1500 rotor and a one-third scale model of the UTRC 8 kW turbine. For the Enertech rotor, experimental data compared well with theory, with the worst error being on the order of 0.04 in power coefficient at a tip speed ratio of 5. The maximum theoretical power coefficient was 0.397, compared to 0.37 for the data. For the UTRC turbine, the data did not compare well with theory. The discrepancy was greatest at a tip speed ratio of 8, where the theory gave a power coefficient of 0.32, but the data gave only 0.21. It was postulated that the discrepancy was due to a source of high rotor drag not identified in the experimental test program.

The overall conclusion is that the model is ready to be used as a design tool, but the user must have a good working knowledge of the two-dimensional aerodynamic characteristics of the blade airfoil to be employed.

EXECUTIVE SUMMARY

The analysis of horizontal axis propellers and turbines has been an area of increased interest in recent years because of the need to develop adequate analytical tools for the design and evaluation of wind turbine rotors. Among industry standards is the PROP computer code developed as a result of the work in the mid-1970s by R.E. Wilson of Oregon State University and P.B.S. Lissaman of AeroVironment Inc. ~~especially for wind turbine analysis~~. The PROP code or modified versions of it have been used successfully in the design of a number of wind turbines, but no comprehensive effort has been made to compare analysis and experimental results, due primarily to the lack of well-documented experimental data for wind turbines.

The purpose of this study was to make improvements in the PROP code, to analyze two existing rotors, to compare analytical results with experimental data, and to make adjustments to the code as required by the comparison of theory and experiment. The approach to the program was to make the performance prediction based only on the technical specification of the rotors. With the analysis completed, Rockwell International Energy Systems Group at Rocky Flats, Colorado, provided test data on the two systems and the comparison between theory and experiment was made. The major items of work and the results and conclusions of the study are summarized below.

Description of the Analytical Model

The basic computer program used was an updated version of the PROP code developed for NASA Lewis Research Center. This program computes horizontal axis windmill performance using Glauert momentum strip theory. The program uses, as input, the twist, chord, and the lift-drag characteristics of the airfoils at several stations along the blade. The specification of the airfoil characteristics at each station allows the inclusion of Reynolds number effects along the blade length. As the blade rotates, each element sweeps out an annular strip. The Glauert strip theory determines the windmill performance by equating the blade forces, both axial and circumferential, determined by two-dimensional airfoil theory, with the change in momentum of the air going through the annular strip. Once the change in the momentum is known, the axial and circumferential interference factors are computed. This allows computation of the flow velocity and angle of attack at the blade element, closing the problem. Typically, the equations describing the above process are solved in an iterative manner.

The complete PROP code was rewritten and the following items summarize the analyses performed and the current status of the code.

1. Prandtl tip loss correction factors for the blade tip and root were included in the original version and were retained in the improved version.

2. Modifications were made to the basic equations to account for operation in the windmill brake state. Two models were developed: (1) an advanced model that uses an approximation to Glauert's empirical relationship between head loss coefficient and axial induction to analyze rotor performance above a head loss coefficient of 1.0, and (2) a classical momentum brake state model which does not permit the head loss coefficient to exceed 1.0.

3. Wind shear effects were included. These were treated by considering the variation of horizontal wind speed at different heights on the rotor disc.

4. An analytical representation for two-dimensional airfoil section characteristics over a wide range of angles of attack was developed. Extrapolation curves were constructed for regions beyond the angle of attack range for which experimental data is normally available.

5. The effects of turbulence and cross-flow were considered for the model but not included. An analysis was made which showed that turbulence effects are negligible for small WECS and that off-axis effects can be handled by a simple power-of-cosine-of-angle relationship.

6. The model was set up so that different airfoil data could be used at each radial station.

Analysis of Specified Rotors

A conventional rotor analysis was conducted of two rotor systems, the Enertech 1500 and a one-third scale model of the UTRC 8 kW turbine. Using airfoil and planform data supplied by Rockwell, performance curves of power coefficient, P_C, versus tip speed ratio, X, were generated for a series of feather angles for three cases: (1) classical brake state model, (2) advanced brake state model, and (3) advanced brake state model with wind shear. The maximum calculated P_C's were 0.40 for the Enertech 1500 and 0.34 for the UTRC 8 kW turbine.

Comparison of Theory and Experiment

Because the test data provided by Rockwell were obtained in no-shear conditions and at tip speed ratios for which the rotors were not operating in brake state, these features of the code could not be checked. Thus, the calculation was made for the theoretically preferred advanced brake state model calculations with no wind shear.

For the Enertech 1500 rotor, the data compared well with theory, with the worst error being on the order of 0.04 in power coefficient at a tip speed ratio of 5. The maximum predicted power coefficient was 0.397, compared to 0.37 for the data. For tip speed ratios less than 4, the comparison was excellent. The discrepancies at higher tip speeds may have been due to errors in the airfoil data used. The prediction was made assuming NACA 4412 and 4415 airfoil data. In actuality, the Enertech rotor does not use this airfoil, but one similar to it.

For the one-third scale UTRC turbine, the data did not compare well with theory. The discrepancy between the two curves was greatest at a tip speed ratio of 8, where theory gave a power coefficient of 0.32, but the data gave only 0.21. This large difference could be accounted for by assuming a large, unidentified source of drag for the turbine blades. If a C_D increment of 0.020 is assumed along the entire blade span at all angles of attack, then the calculated performance is in good agreement with the data. An increase in section drag coefficient of 0.020 is quite large, as it more than doubles the drag. This increase cannot be explained as a low Reynolds number effect because the airfoil data originally used was low Reynolds number data. Premature stall is not a possibility as the

performance loss occurs at high tip speed ratios where the airfoil will not be stalled. The most likely drag source is due to the improper construction of the airfoil section or, as suggested by Rockwell personnel, there may have been aeroelastic deformation of the model under test. It is believed that the one-third scale UTRC model gave such poor performance, with a maximum power coefficient of 0.21, that there had to be some source of high rotor drag not identified in the test program.

Modifications to the Theoretical Model

With the proper selection of airfoil characteristics, it was shown that the theory and data agreed well. However, the airfoil characteristics used in the model for the stalled region are somewhat arbitrary, and a better description of the stalled airfoil characteristics was developed to enable better performance prediction at low tip speed ratios (corresponding to high wind speeds in constant RPM systems, an area where airfoil stall is used to control power output) and starting torque. An empirical modification was made to the stalled flat plate model characteristics in the shallow stall range of angles of attack, 12^{o} to 26^{o}. The resulting modified stalled flat plate model showed much better agreement with the experimental data for the Enertech and UTRC rotors and has been included in the final version of the model.

Conclusions

1. The PROP code in final form with proper airfoil characteristics can be used to calculate rotor performance over a broad range of blade geometries and tip speed ratios.

2. While the model has not been correlated with experiment for wind shear and brake state, primarily because of lack of data, the model has been shown to give excellent agreement with data for the nominal design case of no-shear and no-brake state.

3. The model is ready to be used as a design tool but requires that the user have a good working knowledge of airfoil characteristics so that at the design Reynolds number the appropriate airfoil data is used.

Recommendations

To further improve the accuracy and usefulness of this computer program, the following investigations are recommended:

1. Comparison with rotors operating in wind shear. Experimental rotors should be run in wind shears large enough to cause major changes in performance. Wake surveys should be conducted to ascertain how the blade performance varies about the circumference of the turbine.

2. Brake state model. Experiments are recommended to ascertain the accuracy of the brake state model currently used.

3. Off-axis flow. It is recommended that an experiment be conducted to determine how rotor performance varies in off-axis flow.

4. Airfoil characteristics. More information is needed on airfoil characteristics in the shallow stall regime. Further, it should be determined if these characteristics change in the rotating environment of a turbine blade due to centrifugal or other effects.

TABLE OF CONTENTS

		Page
	ABSTRACT	i
	EXECUTIVE SUMMARY	ii
	TABLE OF CONTENTS	vi
	LIST OF FIGURES	vii
	LIST OF TABLES	viii
1.0	INTRODUCTION	1
2.0	NOMENCLATURE	3
3.0	DESCRIPTION OF ANALYTICAL MODEL	9
3.1	Basic Blade Element Theory	9
3.2	Tip Loss Correction	16
3.3	Brake State Model	17
3.4	Wind Shear Effects	20
3.5	Summary of Equations Used in Computer Model	21
3.6	Representation of Airfoil Characteristics	25
3.7	Centrifugal Effects	25
3.8	Turbulence Effects	25
4.0	INPUT/OUTPUT PARAMETERS FOR THE COMPUTER MODEL	37
5.0	SPECIFIC TURBINE ANALYSIS AND RESULTS	39
6.0	COMPARISON OF THEORY AND EXPERIMENT	41
6.1	Comparison of Data With the Original Prediction	41
6.2	Modifications to the Theoretical Model	42
7.0	RESULTS, CONCLUSIONS AND RECOMMENDATIONS	55
7.1	Results	55
7.2	Conclusions	55
7.3	Recommendations	55
8.0	REFERENCES	57

APPENDICES

A	Computer Calculations for Rotor A and Rotor B
B	User's Manual for the PROP Code

LIST OF FIGURES

Number	Description	Page
1	Rotor geometry	10
2	Velocities and forces on a blade element	11
3	Relation between $\underline{a}$ and C_H in the brake state	19
4	Analysis points for wind shear model	22
5	Representation of airfoil lift and drag coefficient curves	26
6	Spectrum of horizontal gustiness in high winds at 10-m height	27
7	Geometry of cross-flow model	31
8	Torque coefficient of a blade element with a chord of 0.075, two blades, zero feather angle, at a speed ratio of 7	34
9	Torque coefficient of a blade element with a chord of 0.15, two blades, 5 degrees pitch angle, at a speed ratio of 7	35
10	Enertech turbine comparison, original prediction	42
11	UTRC turbine comparison, original prediction	43
12	Airfoil characteristics used in the original prediction	45
13	Normal force coefficient on a stalled flat plate of finite aspect ratio	47
14	Airfoil characteristics, stalled flat plate model	49
15	Enertech turbine comparison with theory, stalled flat plate model used, $\Delta\beta = 0^{\circ}$.	50
16	UTRC turbine comparison with theory, stalled flat plate model used, $\Delta\beta = 0^{\circ}$.	51
17	Airfoil characteristics, modified stalled flat plate model	52
18	Enertech turbine comparison to theory, modified stalled flat plate model	53
19	UTRC turbine comparison to theory, modified stalled flat plate model	54

LIST OF TABLES

Number	Description	Page
I	Turbulence intensity in a 10-meter per second wind at 10 meters altitude	29

1.0 INTRODUCTION

The analysis of horizontal axis propellers and wind turbines has been important for more than a century and numerous theories and correction factors have been proposed over the years. Wilson and Lissaman (1974)[1] and, more recently, de Vries (1979)[2] give a good discussion of general momentum theory applied to an actuator disc with power extraction and of vortex/strip (blade element) theory applied to windmill analysis. The blade element theory, in which the aerodynamic forces on each element are equated to the change in momentum in the annulus swept by the element to determine the aerodynamic interference (swirl and axial retardation), is used as the basis for the Wilson-Lissaman windmill analysis computer program which is widely used in the industry today. This method is rapid and effective but fails in the overload or windmill brake state. There is also uncertainty about two-dimensional airfoil characteristics and about the tip loss corrections. In spite of the above deficiencies, this model has many desirable features, and with some judicious tuning, it is probably as good as can be justified for design and performance estimation of practical wind turbines.

The basic computer program used is an updated version of the PROP code developed by NASA Lewis Research Center (Wilson et al., 1976)[3]. This program computes horizontal axis windmill performance using Glauert momentum strip theory. The program uses, as input, the twist, chord, and the lift-drag characteristics of the airfoils at several stations along the blade. The specification of the airfoil characteristics at each station allows the inclusion of Reynolds number effects along the blade length. As the blade rotates, each element sweeps out an annular strip. The Glauert strip theory determines the windmill performance by equating the blade forces, both axial and circumferential, determined by two-dimensional airfoil theory, with the change in momentum of the air going through the annular strip. Once the change in the momentum is known, the axial and circumferential interference factors are computed. This allows computation of the flow velocity and angle of attack at the blade element, closing the problem. Typically, the equations describing the above process are solved in an iterative manner.

Several program modifications to this analysis may be used to increase the accuracy of the method. One improvement is the use of optional tip loss corrections already in the computer code. Near the ends of the blades, both at the hub and at the tip, a vortex is shed. The local induced flow caused by this vortex is greater than the value given by the basic Glauert theory, which assumes a tubular sheet of vorticity. This increase in induced flows can be modeled by the Prandtl tip loss equations, and will depend on given rotor geometry.

Another program modification is the inclusion of wind shear. Wind shear can be treated by analyzing the blade performance at several circumferential positions, using the local wind speed for each element at each position. Thus, the average blade performance can be calculated.

For computations in the windmill brake state, standard momentum theory lacks a relation between the axial interference factor and the axial thrust coefficient, which is identical to the head loss coefficient, that is valid for thrust coefficients greater than 1.0. Experimental data has shown that windmills can operate at thrust coefficients of up to 2.0. Glauert used this data to develop an empirical relation for large thrust coefficients.

Using this relation, it is possible to estimate the performance in the brake state using no more computer time than normal for windmill analysis. AeroVironment Inc. has successfully used this empirical relation to predict the maximum possible performance of augmented windmills where very high thrust coefficients occur.

In this report, modifications to the computer code are discussed and a number of aerodynamic effects on rotor performance are discussed. Chapter 3 discusses the analytical model and the development of the equations used. The equations have been developed and are given in a form amenable to the computer code. The following subjects have been treated in the analysis:

1. Development of the basic blade element theory equations for thrust, torque, and power for a given annulus.

2. Inclusion of the Prandtl tip loss correction factors for the blade tip and root.

3. Modifications of the basic equations to account for operation in the windmill brake state. Two models have been developed: (1) an advanced model that uses an approximation to Glauert's empirical relationship between head loss coefficient and axial induction to analyze rotor performance above a head loss coefficient of 1.0, and (2) a classical momentum brake state model which does not permit the head loss coefficient to exceed 1.0.

4. Wind shear effects. These have been treated in terms of the variation of axial wind speed observed at different heights on the rotor disc.

5. The equations used in the model have been summarized.

6. A representation for two-dimensional airfoil section characteristics. Extrapolation curves are given for regions beyond the normal angle of attack range.

7. Centrifugal effects. These are mentioned, but are not understood well enough or supported by data to be included in analytical form in the model.

8. The effects of turbulence and cross-flow. An analysis has been made which shows that these effects should be quite small for small WECS.

In Chapter 4, the input and output parameters for the computer program are given.

In Chapter 5, the analysis conducted on the two turbine designs, turbines A and B, are described.

Chapter 6 compares performance data with the original prediction. Results, conclusions, and recommendations are presented in Chapter 7. Chapter 8 cites the references.

Curves of power coefficient versus tip speed ratio are given in Appendix A for the various cases analyzed as are support data on blade lift distribution and performance. The results of the analysis are also discussed.

Appendix A gives rotor performance calculations, and Appendix B is a user's manual for the PROP code.

2.0 NOMENCLATURE

The following symbols, definitions, and conventions have been used throughout this report.

a	Axial interference factor at the plane of the rotor, plus a is a reduction in flow speed so that, $V_{axial} = V_o (1 - a)$
a'	Circumferential interference factor at the plane of the rotor, plus a' is an increase in circumferential velocity due to swirl so that, $V_C = R\Omega a'$
a_c	Cross-flow interference factor at the plane of the rotor, plus a_c is a reduction in cross-flow velocity so that, $V_0 V_c (1 - a_c)$
B	Number of blades
C	Blade chord at any radial station
C_D	Two-dimensional airfoil drag coefficient, $\frac{D}{1/2 \rho W^2 C}$
C_H	Head loss coefficient, $\frac{\text{head loss across rotor}}{q_0 S_{disc, proj}}$, this is equal to the normalized axial momentum change through the rotor i.e., $C_H = 4a(1 - a)$ for this analysis
C_L	Two-dimensional airfoil lift coefficient, $\frac{L}{1/2 \rho W^2 C}$
C_M	Mass flow coefficient, $\frac{M}{S_d V_0}$
C_n	Coefficient of force normal to airfoil chord line
C_P	Coefficient of power, $\frac{P}{n^3 (2R_T \cos \psi)^5}$
C_Q	Coefficient of torque, $\frac{Q}{n^2 (2R_T \cos \psi)^4}$

C_t Coefficient of force tangential to airfoil chord line

C_T coefficient of thrust, $\dfrac{T}{n^2 (2R_T \cos\psi)^4}$

D Blade element drag, parallel to blade element incident velocity, W, or rotor diameter

E Velocity shear profile exponent

F Combined tip loss correction, $F = F_H F_T$

F_C Cross-flow force on a blade element

F_H Hub loss correction

F_T Tip loss correction

f Prandtl tip loss correction exponent

H_O Rotor hub height

H_L Local height of a blade element at some circumferential position

I Turbulence intensity

J Advance ratio, $\dfrac{V_o}{n^2 R_T \cos\psi}$

K Ground surface drag coefficient used in computing turbulence spectral density

L Blade element lift, normal to blade element incident velocity, W

L_N Normal component of L (normal to projected rotor disc)

L_C	Cross-flow component of L (in direction of cross flow velocity, V_c)
n	Frequency of turbulence, Hz, or rate of rotation, Hz,
p	Pressure
P	Power
P_C	Power coefficient, $\frac{P}{q_0 V_0 S_d}$
q_0	Free stream dynamic pressure, $1/2\,\rho V_0^2$
Q	Torque
Q_C	Torque coefficient, $\frac{Q}{q_0 S_d R_T}$
R	Radius along blade to any blade element
Re	Reynolds number
R_H	Radius along blade to hub end of blade
R_T	Radius along blade to tip of blade
S_w	Algebraic group defined in text
S(n)	Spectral density of turbulence
S_a	Projected area of any annulus
S_d	Projected area of the entire rotor disc, $\pi R_T^2 \cos^2\psi$
T	Thrust in downstream direction

T_C Thrust coefficient, $\frac{T}{q_0 S_d}$

V_c Cross-flow velocity component normalized to V_0, i.e., $V_{cross\text{-}flow}/V_0$

V_L Local freestream velocity for an annulus segment with blade element at height H_L,

V_n Normal (axial) velocity component normalized to V_0, i.e., V_{normal}/V_0

V_0 Freestream velocity

W Local incident velocity on a blade element, computed in plane normal to the leading edge of the element so that two-dimensional airfoil characteristics can be normalized to this velocity

X Tip speed ratio, $R\Omega\cos\psi/V_0$

X_n X/V_n

x Wave number

x_1, x_2 Range of wave numbers of interest

X_L Local tip speed ratio based on V_L, $R\Omega\cos\psi/V_L$

Subscripts

$(\ )_{blade\ element}$ Quantity applies to calculations performed on a blade element

$(\ )_{momentum}$ Quantity applies to calculation of momentum change in a blade element annulus

$(\ )_\ell$ Local coefficient referenced to annulus projected area

$( )_L$	Local coefficient referenced to the blade element conditions at height H_L
$( )_{wake}$	Quantity applies to calculations made in the wake, far downstream of the rotor

Greek symbols

α	Local angle of attack of any blade element
θ	Circumferential angle measured from vertical
γ	Cross-flow angle
$\Delta( )$	Incremental value, small but finite quantity
ρ	Density of air
σ	Rotor solidity ratio
φ	Relative wind velocity angle for a blade element, measured from the plane of the rotor to the velocity vector, W. Note that this angle is actually measured from a reference plane tangent to the cone of rotation for a coned rotor
ψ	Coning angle
Ω	Rotational speed
β	Angle measured from reference plane of rotation to the chord line of a blade element when the feather angle $\Delta\beta = 0$. The distribution of β along the blade defines the twist of the rotor blade
$\Delta\beta$	Feather angle caused by a rigid blade pitch rotation of all blade elements. $\beta + \Delta\beta$ is the angle between the reference rotational plane and the chord of a blade element at this feather angle

Notes on Nomenclature

The PROP program is designed to handle both wind turbines and propeller rotors. Unfortunately, the standard definition of C_p for propellers is not the same as the one used for wind turbines. For propellers, C_p is found by normalizing power by $\rho n^3 D^5$, where ρ is the density, n is the rate of rotation in cycles per second, and D is the diameter. For wind turbines, the normalizing factor is $1/2\rho V_0^3 \pi R_T^2$.

In propeller nomenclature, both definitions are used. However, the wind turbine definition is given the variable name, P_c. It was decided to adopt this form for the nomenclature. It was found that the propeller definition, C_p, had utility in wind turbine work. This is because most modern turbines operate at constant rpm. Hence, the normalizing factor is a constant and C_p is proportional to power.

Another useful variable normally used for propellers is the advance ratio, J, defined as $J = V_0/nD$. J is thus proportional to V_0 in a constant rpm system. Thus, a curve of C_p versus J is simply a normalized form of the power versus wind speed curve of the turbine. The current form of PROP outputs both C_p and P_c as well as X and J. Provisions have been made to analyze the rotor at equal increments in either X or J, as the user wishes.

3.0 DESCRIPTION OF ANALYTICAL MODEL

3.1 Basic Blade Element Theory

A horizontal axis wind turbine may be analyzed by the same methods used to analyze propellers. One effective and accurate method is called blade element or strip theory. The rotor blade is divided up into a number of spanwise elements or strips at radial stations along the blade. Each of these elements sweeps an annulus as the blade rotates. The axial and tangential velocity interference terms, $\underline{a}$ and $\underline{a}'$, are determined by equating the forces on each blade element with the change in momentum of the fluid flowing through the annulus swept by that element. It is one of the assumptions of strip theory that the various annuli cannot interfere with each other. Another is that the forces on each blade element are due entirely to the lift and drag forces on the element and these forces are the only ones that influence the flow through the annulus. It is also assumed that the annulus flow is steady and axisymmetric, so that the existence of discrete rotor blades is not specifically taken into account, except for the tip effect.

Figure 1 shows the turbine with the blades coned at an angle of ψ. The length of each blade is R_T. Because the blade is coned, the radius of the projected swept rotor disc is $R_T \cos\psi$, giving a projected swept area of $\pi R_T^2 \cos^2\psi$. It is this area to which the turbine thrust, torque, and power coefficients are normalized. A blade element has a radius R and a width ΔR. The area of the element is thus $C\Delta R$ where C is the chord of the blade at the element. The projected area is $C\Delta R \cos\psi$. The projected width of the swept annulus is $\Delta R \cos\psi$, giving a swept area of $2\pi R \Delta R \cos^2\psi$. The solidity, σ, of the strip is equal to the ratio of the area of the blades to the swept area. For an annulus this is

$$\sigma = \frac{BC}{\pi R \cos\psi}$$

where B is the number of blades.

The tip speed ratio of the turbine, X, is defined as the ratio of the speed of the turbine blade tip to the free wind speed, V_0, thus:

$$X = \frac{\Omega R_T \cos\psi}{V_0}$$

where Ω is the blade rotation rate. Figure 2 shows the flow velocities and forces as seen by a blade element at radius R. The relative flow velocity, W, is

$$W = \sqrt{V_0^2(1 - a)^2 \cos^2\psi + (1 + a')^2 \Omega^2 R^2 \cos^2\psi}$$

which can be reduced to

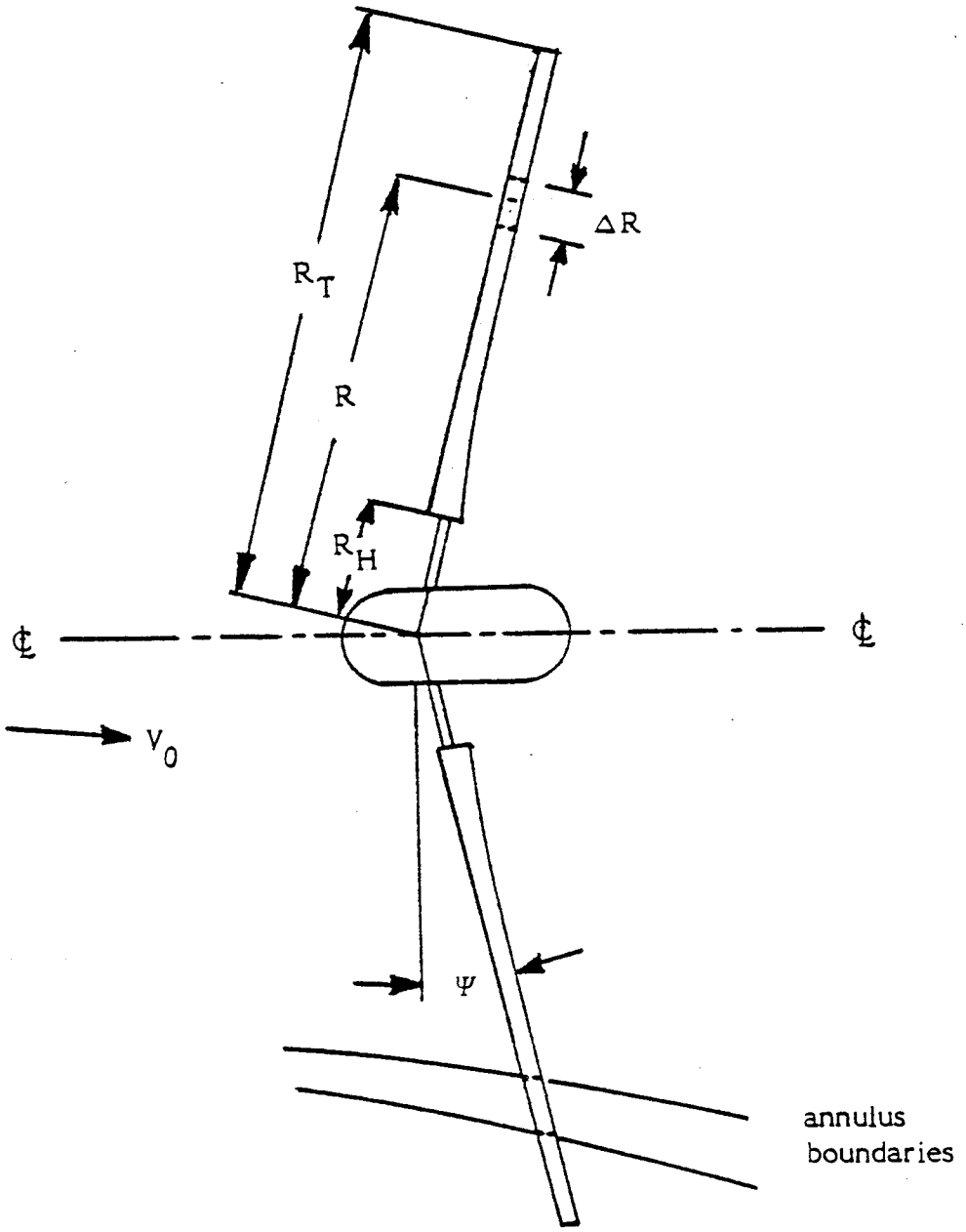

FIGURE 1. Rotor geometry.

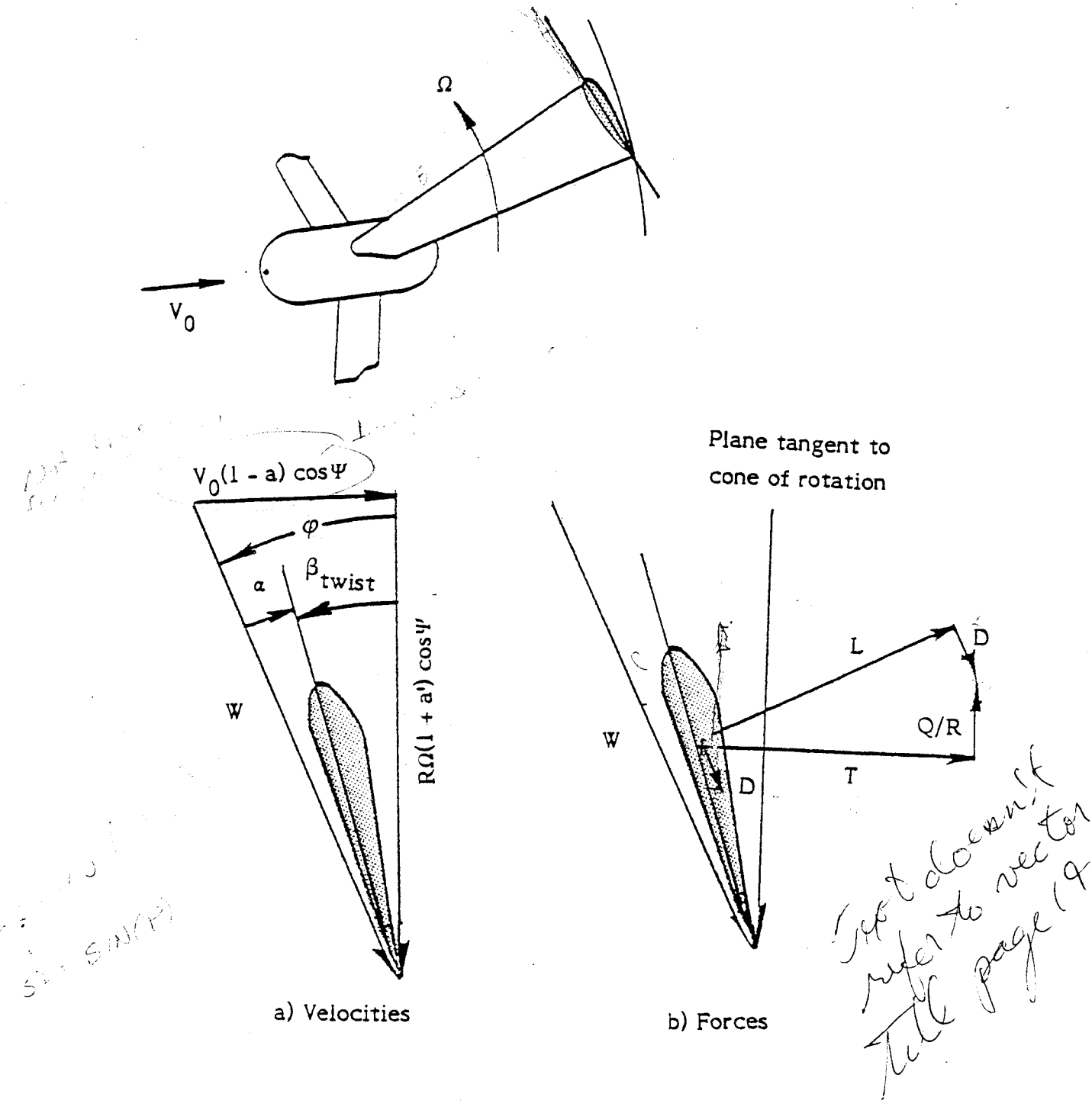

FIGURE 2. Velocities and forces on a blade element.

$$W = V_0 \sqrt{(1 - a)^2 \cos^2 \psi + (1 + a')^2 X^2 \left(\frac{R}{R_T}\right)^2}$$

or can be put in terms of the incoming flow angle, φ, as

$$W = V_0 \frac{(1 - a) \cos \psi}{\sin \varphi}$$

where the angle of the incoming flow to the plane of rotation, φ, is

$$\varphi = \text{atan} \frac{V_0(1 - a)}{R\Omega(1 + a')} = \text{atan} \frac{R_T}{R} \frac{(1 - a) \cos \psi}{X (1 + a')}$$

It is now possible to write the equations for the forces on the blade and the change of momentum of the fluid flowing through the annulus. There are two sets of equations to be considered, one for the axial forces and momentum, and one for the tangential forces and momentum.

o Blade Element Axial Force Equation

To find the axial interference factor, a, it is necessary to equate the axial forces on the blade element to the momentum change in the annulus. The force on a blade element of width, ΔR, is equal to

$$\text{axial blade force} = \frac{1}{2} \rho W^2 C \Delta R (C_L \cos \varphi + C_D \sin \varphi)$$

Only part of this force acts in the downstream direction due to the rotor coning. Also, this force must be multiplied by the number of blades, B. The incremental thrust on the blades in a particular annulus is thus

$$\Delta T = \frac{1}{2} \rho W^2 BC \Delta R (C_L \cos \varphi + C_D \sin \varphi) \cos \psi$$

This is equal to the change in momentum of the flow through the annulus, or the pressure drop across the rotor times the annulus area. The pressure drop, ΔP, is

$$\Delta P = \frac{1}{2} \rho V_0^2 C_H$$

giving for ΔT,

$$\Delta T = \frac{1}{2} \rho V_0^2 C_H (2\pi R \Delta R \cos^2 \psi)$$

Equating these two equations, canceling like terms, and making some substitutions,

$$V_0^2(2\pi R)\, C_H \cos^2\varphi = W^2\, BC(C_L \cos\varphi - C_D \sin\varphi)\cos\psi$$

$$C_H = \frac{W^2}{V_0^2}\,\frac{BC}{2\pi R}\,\frac{(C_L\cos\varphi + C_D\sin\varphi)}{\cos\psi}$$

$$C_H = \frac{\sigma}{2}\,\frac{(1-a)^2\cos^2\psi}{\sin^2\varphi}\,(C_L\cos\varphi + C_D\sin\varphi)$$

The head loss coefficient can be related to a via momentum theory:

$$C_H = 4a(1-a) \quad \text{and} \quad a = \frac{1-\sqrt{1-C_H}}{2}$$

At this point, it is convenient to assume that the lift force is the only force that causes changes in the flow velocity in the annulus. The drag of the blade does indeed cause a flow velocity change, but the effect is limited to a thin sheet containing the wake of the blade and does not change the average flow velocity outside that wake. This is because the drag term does not cause the shedding of an intense helical blade-tip vortex as does the lift term. It is this helical tip vortex which is able (through the Biot-Savart Law) to influence the flow field at points remote from itself. Thus, at this level of approximation, the C_D term may be ignored in the calculation of a. We can now solve for a:

$$4a(1-a) = \frac{\sigma}{2}\,\frac{(1-a)^2\cos^2\psi}{\sin^2\varphi}\,C_L\cos\varphi$$

$$a = \frac{1-\sqrt{1-\frac{\sigma}{2}\,\frac{(1-a)^2\cos^2\psi}{\sin^2\varphi}\,C_L\cos\varphi}}{2}$$

Note that $a(1-a)^2$ term is still contained in the right side of the equation. It is desirable to leave the equation in this form to simplify t… In any case, the equation will have to be solved … left side being the new a of each iteration.

o Blade Element Tangential Force Equation

The circumferential interference factor, a', is … generated by the blade element, with the chang… The torque is equal to the component of the bla… which for a single blade element of width ΔR is …

$$\text{circumferential blade force} = \frac{1}{2}\rho W^2 C\Delta R (C_L \sin\varphi - C_D \cos\varphi)$$

multiplied by the moment arm length, R cos ψ, and by the number of blades, B, giving ΔQ for a particular annulus as,

$$\Delta Q = \frac{1}{2}\rho W^2 BC\Delta R(C_L \sin\varphi - C_D \cos\varphi) R \cos\psi$$

Again, only the lift of the blade will be considered in the computation of a'. This torque is equal to the amount of angular momentum added to the air. This can be determined by multiplying the total circumferential velocity added to the annulus, times the mass flow of the annulus.

The total circumferential velocity added is the circumferential velocity downstream of the rotor, which is twice the circumferential velocity at the rotor,

$$\text{downstream circumferential velocity} = 2R\Omega a' \cos\psi$$

With the annulus mass flow given by

$$\text{mass flow} = \rho V_0 (1 - a) 2\pi R\Delta R \cos^2\psi$$

the incremental angular momentum is then,

$$\Delta Q = 4\pi\rho V_0 R^2\Delta R (1 - a) a'\Omega\cos^3\psi$$

Equating the two relations and simplifying,

$$4\pi\rho V_0 R^2\Delta R(1 - a) a'\Omega\cos^3\psi = \frac{1}{2}\rho W^2 BC\Delta R(C_L \sin\varphi) R \cos\psi$$

$$8\pi V_0 R\Omega(1 - a) a' \cos^2\psi = W^2 BC (C_L \sin\varphi)$$

From Figure 2 we have;

$$\sin\varphi = \frac{(1 - a)V_0 \cos\psi}{W}$$

and;

$$\cos\varphi = (1 + a') \frac{R\Omega\cos\psi}{W}$$

substituting in these relations as well as the relation for σ;

$$\frac{a'}{1 + a'} = \frac{\sigma C_L}{8 \cos \varphi}$$

The equations for $\underline{a}$ and $\underline{a}'$ must be solved in an iterative manner. The procedure used is:

1. Define the geometry of the turbine by specifying blade chord, twist, cone, tip speed ratio, and 2-D airfoil section characteristics.

2. Assume initial values for $\underline{a}$ and $\underline{a}'$ (zero is an acceptable initial assumption) for a given station.

3. Calculate W, φ, and the airfoil angle of attack, α.

4. Using the blade 2-D airfoil section characteristics, find C_L.

5. Using the above momentum balance equations, determine new $\underline{a}$ and $\underline{a}'$.

6. Compare these new values with the previous iteration values. If the difference is within a certain preset magnitude, stop iteration and go to the next blade element; otherwise iterate as described in step 7.

7. Find a new estimate for $\underline{a}$ and $\underline{a}'$, and go back to step 3. There are several methods for finding the new estimate for $\underline{a}$ and $\underline{a}'$. One is to use those values determined in step 5. Another is to average the values found in step 5 with those used at the start of the iteration. In practice, neither of these methods is unconditionally convergent. It has been found, however, that if the assumed values for $\underline{a}$ and $\underline{a}'$ are incremented by small amounts toward the values found in step 5, with the increment being decreased whenever the direction of incrementation is reversed, then the method will converge.

Once $\underline{a}$ and $\underline{a}'$ have been found, the annulus values for the torque, thrust, and power coefficients, ΔQ_C, ΔT_C, and ΔP_C, may be found. When normalized to the projected area of the annulus, thus giving the local values, Q_{C_ℓ}, T_{C_ℓ} and P_{C_ℓ}, these are:

$$Q_{C_\ell} = \frac{B}{2\pi \cos^2 \psi} \frac{C}{R_T} \left[(1 - a)^2 \cos^2 \psi + (1 + a')^2 X^2 \left(\frac{R}{R_T} \right)^2 \right] (C_L \sin \varphi - C_D \cos \varphi)$$

$$T_{C_\ell} = \frac{B}{2\pi \cos \psi} \frac{C}{R} \left[(1 - a)^2 \cos^2 \psi + (1 + a')^2 X^2 \left(\frac{R}{R_T} \right)^2 \right] (C_L \cos \varphi + C_D \sin \varphi)$$

$$P_{C_\ell} = X Q_{C_\ell}$$

The values for ΔQ_C, ΔT_C, and ΔP_C are equal to the local values times the ratio of the area of the annulus to the entire rotor. For example,

$$\Delta Q_C = Q_{C_\ell} \frac{2R\Delta R}{R_T^2}$$

The other equations are similar.

3.2 Tip Loss Correction

The basic analysis presented above does not take into account the aerodynamic losses caused by vortices shed from the tips of finite blades. A tip loss correction is required by the fact that there are a finite number of blades of finite tip chord while blade element theory implies an infinite number of vanishingly small blades. Tip loss correction is important because tip losses can cause a decrease in torque and, hence, power output from the blade. Thus, it is necessary to examine the properties of tip loss and how it can be modeled.

The standard strip theory, as described, assumes that the flow through each annulus is uniform. In fact, each blade sheds a discrete vortex near the tip. The effect of this helical vortex is to produce an induced flow field which is not uniform, but varies around the annulus, with a period related to the number of blades. This causes an increase in both the axial and circumferential interference factors in the vicinity of the blade tip. This causes a decrease in section angle of attack, as well as a decrease in the circumferential component of the lift force, resulting in decreased torque. The effect is greatest for blade elements near the tip, and decreases for inner elements. The effect is also smaller if the helix formed by the vortices is tighter, which occurs when the tip speed ratio is increased. This would also be the case if the number of blades are increased, causing the flow more nearly to approach blade annulus theory.

A good approximation to the tip loss is given by the Prandtl model (Durand, 1934)[4]. This model is a close approximation to the actual loss factor. The formulas used are simple and have been used with good success. The Prandtl tip loss factor, F_T, is

$$F_T = \frac{2}{\pi} \arccos\left(e^{-f}\right)$$

where

$$f = \frac{B}{2} \frac{R_T - R}{R_T \sin\varphi_T}$$

In the expression for f, the factor, $R_T \sin\varphi_T$, can be approximated by $R \sin\varphi$, which is more easily computed.

If the blade ends before reaching the hub, then there will be a hub loss factor, F_H, similar to the tip loss factor. The equation for F_H will be the same as for F_T, but f is now;

$$f = \frac{B}{2} \frac{R - R_H}{R_H \sin\varphi}$$

where R_H is the radius of the hub. The total loss factor, F, is simply the product of F_T and F_H, or

$$F = F_T F_H$$

The loss factor can now be applied to the equations for $\underline{a}$ and $\underline{a}'$. The flow velocity components through the annulus averaged around the annulus are less by the factor F. An examination of the equation for F reveals that F has a value approaching 1.0 far from the tip, decreasing to zero at the tip. Because the average flow velocity (again, averaged around the annulus) determines the rate of momentum transfer to the air, the annulus equation for $\underline{a}$ becomes:

$$4aF(1-aF) = \frac{\sigma}{2} \frac{(1-a)^2 \cos^2\psi}{\sin^2\varphi} C_L \cos\varphi$$

or

$$a = \frac{1 - \sqrt{1 - \frac{\sigma}{2} \frac{(1-a)^2 \cos^2\psi}{F \sin^2\varphi} C_L \cos\varphi}}{2F}$$

and for $\underline{a}'$:

$$\frac{Fa'}{1+a'} = \frac{\sigma C_L}{8 \cos\varphi}$$

These equations are solved using the same iterative procedure outlined above.

3.3 Brake State Model

o Advanced Brake State Model

The simple blade element model developed exhibits singular behavior when $\underline{a}$ exceeds 0.5. At this level of interference in an ideal inviscid flow, the flow far downstream in the wake would develop a negative value. This means the flow would have reversed and would be approaching the turbine from downstream in the wake. Momentum theory for an actuator disc gives a value for C_H that is less than 1 at this point. In fact, simple inviscid momentum theory can never give a value for C_H exceeding unity, as is implied by a reversed flow state. Experimental data does however, give values of C_H that exceed 1 when $\underline{a}$ is greater than 0.5. This state, known as the brake state, involves significant viscous interaction and cannot yet be treated rigorously. This is because momentum theory does not take into account the turbulent mixing that occurs in the wake. This mixing is not important at values of $\underline{a}$ less than 0.5, as the wake flow field is not radically modified by this mixing.

In both the viscid and inviscid cases, the wake flow simply proceeds downstream. However, when $\underline{a}$ is greater than 0.5, then turbulent mixing is important as the entrainment of the outer flow can prevent the wake flow reversal from occuring, thus

substantially altering the flow field. This radical modification to the flow field must be accounted for if operation in the brake state is to be properly modeled.

Figure 3 shows the relation between $\underline{a}$ and C_H according to momentum theory, and various real experimental data points and curves derived by Glauert. For the purposes of this model, it was decided to approximate the relation between $\underline{a}$ and C_H with a quadratic:

$$C_H = 0.889 - 0.444a + 1.556a^2$$

This quadratic closely approximates Glauert's empirical formula. This relation gives the same value as momentum theory when $\underline{a}$ is 0.4, as well as the same slope of the curve. At $\underline{a}$ equal to one, the relation yields a C_H of two. Solving for $\underline{a}$:

$$a = 0.143 + \sqrt{0.0203 - 0.6427(0.889 - C_H)}$$

When tip loss effects are included, it is necessary to substitute $\underline{a}F$ for $\underline{a}$, thus giving

$$C_H = 0.889 - 0.444aF + 1.556a^2F^2$$

and

$$a = \frac{0.143 + \sqrt{0.0203 - 0.6427(0.889 - C_H)}}{F}$$

This relation is used to solve for $\underline{a}$ whenever C_H is greater than 0.96. Below $C_H = 0.96$, standard momentum theory as represented by the equations given previously will suffice. As before, these equations must be solved iteratively because C_H and $\underline{a}$ are not independent variables.

o Classical Momentum Brake State Model

Another prediction of brake state performance can be found by solving:

$$4aF(1 - aF) = \frac{\sigma}{2} \frac{\cos^2\psi}{\sin^2\varphi} C_L \cos\varphi \, (1-a)^2 \varphi$$

This is the annulus axial momentum balance with the term $(1 - a)^2$ added on the right-hand side. This can be solved iteratively by rearranging the equation as follows:

$$S_w = \frac{\sigma}{2} \frac{\cos^2\psi}{\sin^2\varphi} C_L \cos\varphi$$

giving,

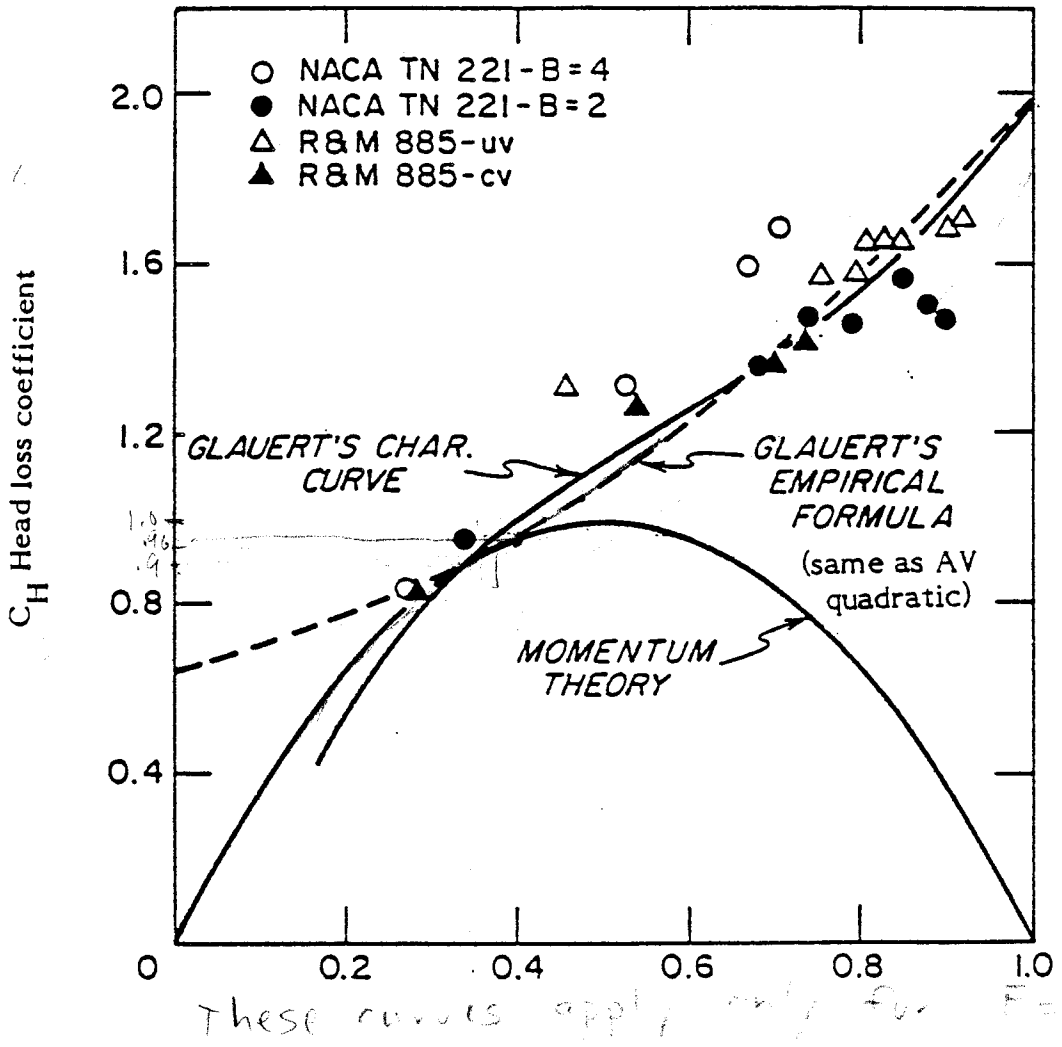

FIGURE 3. Relation between a and C_H in the brake state.

$$a = \frac{2S_w + F - \sqrt{F^2 - 4S_w F(1-F)}}{2(S_w + F^2)}$$

Use of this relation for $\underline{a}$ in the iteration procedure will result in values for $\underline{a}$ and C_H that agree with classical momentum theory at all values of $\underline{a}$, as shown in Figure 3. It should be noted that when $\underline{a}$ is less than 0.4, both relations will give the same value for $\underline{a}$ at the end of the iteration procedure. Both of these equations are included in the computer model.

3.4 Wind Shear Effects

Wind turbines are subject to a wind shear from the atmospheric boundary layer. This can cause changes in the performance of the blade element as it proceeds around its path, as well as changes in the average performance. However, because the magnitude of the wind shear is normally small (say, 17% wind speed change across the rotor for a rotor diameter equal to hub height for a wind profile exponent of 0.167), one would expect the total performance to change by a very small amount. The case for a small performance change can also be made as follows:

Consider a graph of the power output of a blade element as a function of wind speed with the blade element rotating at a constant rate. Over any small range of wind speeds, the power output can be approximated by a linear function of wind speed. If we approximate both the wind shear, as seen by the blade element, and the power versus wind speed curve as linear functions, then it immediately follows that the wind speed and power output of the element will vary as a sine wave with time. For many wind turbines, the experimental power curve is much closer to a linear function than a cubic function. The average speed seen by the element will be equal to the hub height value, and the average power output will be equal to what would be output if the blade element was subjected to the hub height wind speed. Thus, with the above assumptions, wind shear causes no performance change.

In actuality, neither the wind shear nor the power curve are linear functions. Thus, some performance change may be expected. It is necessary to use blade element theory to determine what these changes are for any particular turbine.

The analysis will be done as before, by equating the blade forces to the momentum changes in the annulus. This time, however, the analysis will be carried out over several different circumferential stations about the annulus with the circumferential angle, θ, measured from vertical.

The width of the annular station will be $\Delta\theta$, where

$$\Delta\theta = \frac{2\pi}{N_s}$$

where N_s is the number of circumferential stations. The thrust on an annulus is

$$\Delta T = \frac{1}{2}\rho W^2 \frac{\Delta\theta B}{2\pi} C\Delta R \, (C_L \cos\varphi) \cos\psi$$

Note that $\Delta\theta B/2\pi$ is the number of blades appearing in that particular circumferential section.

The change in flow momentum expressed in terms of the head loss coefficient is

$$\Delta T = \frac{1}{2}\rho V_0^2 (2\pi R \Delta R) C_H \frac{\Delta\theta}{2} \cos^2\psi$$

Note that these two equations are exactly the same as before, except for a $\Delta\theta/\sigma\pi$ term in both components, which can be cancelled when the components are equated. Thus, the final form of the equation for $\underline{a}$ will be the same as before, as will be the equations for $\underline{a}'$, T_C, Q_C, and P_C. All these equations will be normalized to the local velocity, i.e., the flow speed as seen by the station, V_L.

The formula for wind speed as a function of height is

$$V_L = V_0 \left(\frac{H_L}{H_0}\right)^E$$

where V_0 is the wind speed at height H_0, V_L is the speed at height H_L, and E is the wind profile exponent. H_0 will be chosen as the rotor hub height, and will be normalized to the rotor radius. The position of any station will be specified by its radius and its angle θ, from vertical. The height of this point is:

$$H_L = H_0 + R\cos\theta$$

and the speed is

$$V_L = V_0 \left(1 + \frac{R}{H_0}\cos\theta\right)^E$$

The computer program calculates the thrust, torque, and power coefficients of each annular and circumferential section, normalizes these values to the hub velocity, and does a summation to obtain the averaged values for the entire rotor. It is only necessary to find the performance over half the circle; the other half will be the same. The station taken for each section is circumferentially midway between the sides of the section, as shown in Figure 4. In practice, it has been found that three to four sections per half annulus give results of sufficient accuracy; that is, there is no variation in the average values if more sections are taken.

3.5 Summary of Equations Used in Computer Model

For convenience, all the equations used in the computer model are summarized below:

Solidity:

$$\sigma = \frac{BC}{\pi R \cos\psi}$$

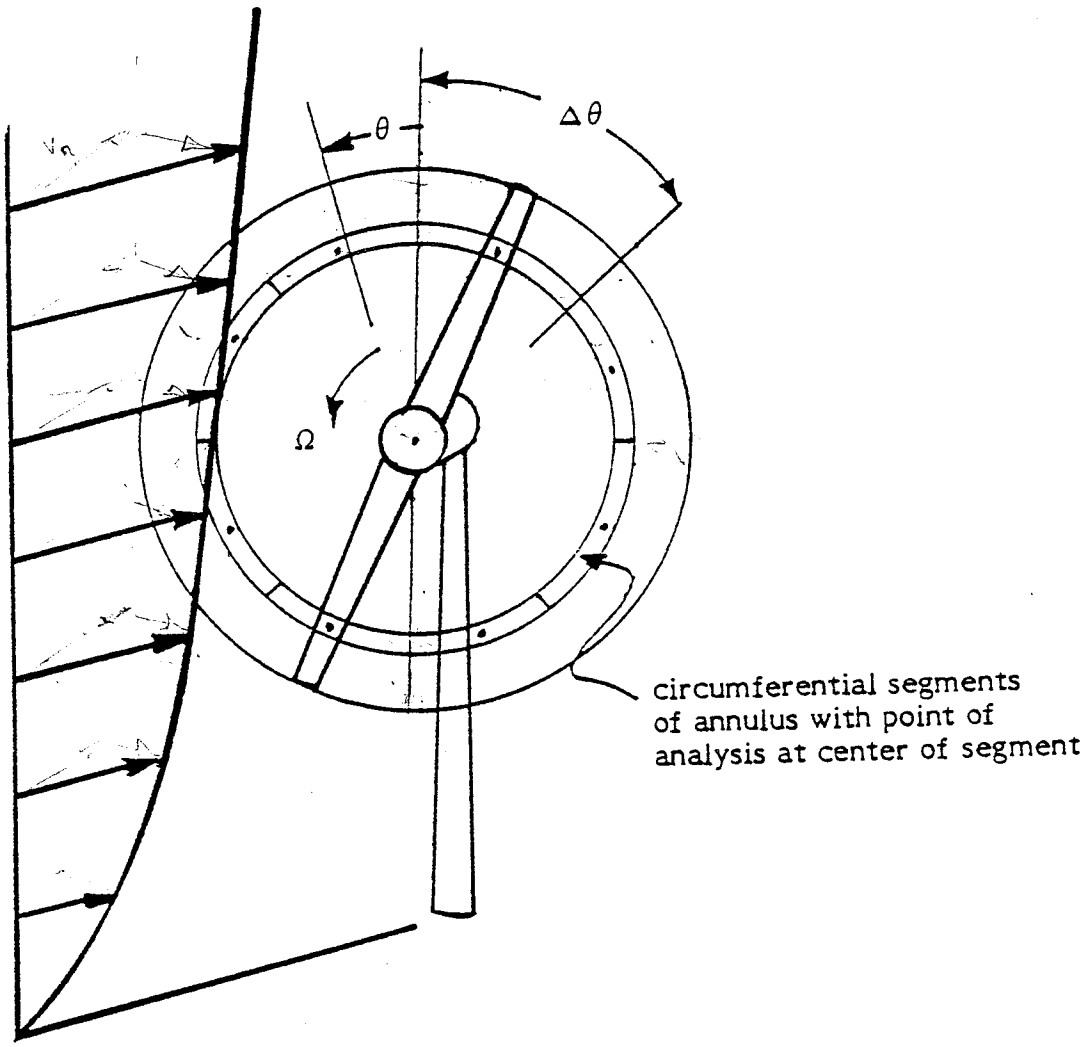

FIGURE 4. Analysis points for wind shear model.

Tip speed ratio: $$X = \frac{R_T \Omega \cos\psi}{V_0}$$

Local flow velocity: $$V_L = V_0 \left(1 + \frac{R}{H_0} \cos\theta\right)^E$$

Local tip speed ratio: $$X_L = X \frac{V_0}{V_L}$$

Flow velocity as seen by blade element: $$W = V_L \sqrt{(1 - a)^2 \cos^2\psi + (1 + a')^2 X_L^2 \left(\frac{R}{R_T}\right)^2}$$

or $$W = V_L \frac{(1 - a)\cos\psi}{\sin\varphi}$$

Incoming flow angle: $$\varphi = \text{atan} \frac{R_T}{R} \frac{(1 - a)\cos\psi}{X_L (1 + a')}$$

Tip loss factor: $$F = \frac{2}{\pi} \arccos(e^{-f})$$

where f at tip is $$f = \frac{B}{2} \frac{R_T - R}{R \sin\varphi}$$

and f at hub is $$f = \frac{B}{2} \frac{R - R_H}{R_H \sin\varphi}$$

o Equations for a:

Classical momentum theory with brake state:

$$S_w = \frac{\sigma}{2} \frac{\cos^2\psi}{\sin^2\varphi} C_L \cos\varphi$$

$$a = \frac{2S_w + F - \sqrt{F^2 - 4S_w F(1 - F)}}{2(S_w + F^2)}$$

advanced brake state theory: $$C_H = \frac{\sigma}{2} \frac{(1-a)^2 \cos^2\psi}{\sin^2\varphi} C_L \cos\varphi$$

C_H less than 0.96: $$a = \frac{1 - \sqrt{1 - C_H^2}}{2F}$$

C_H greater than 0.96: $$a = \frac{0.143 + \sqrt{0.0203 - 0.6427\,(0.889 - C_H)}}{F}$$

o Equation for a':

$$\frac{a'}{1-a'} = \frac{\sigma C_L}{8F \cos\varphi}$$

The local torque, thrust, and power coefficients, normalized to the hub height wind speed, are:

$$Q_{C_\ell} = \frac{B}{2\pi \cos^2\psi} \frac{C}{R_T} \left(\frac{V_L}{V_0}\right)^2 W^2 \,(C_L \sin\varphi - C_D \cos\varphi)$$

$$T_{C_\ell} = \left(\frac{B}{2\pi \cos\psi} \frac{C}{R}\right) \left(\frac{V_L}{V_0}\right)^2 W^2 \,(C_L \cos\varphi + C_D \sin\varphi)$$

$$P_{C_\ell} = X\, Q_{C_\ell}$$

The incremental contributions to the total torque, thrust, and power coefficients from the local values computed at a number of circumferential stations are:

$$\Delta Q_C = Q_{C_\ell} \frac{2R\Delta R\Delta\theta}{\pi R_T^2}$$

$$\Delta T_C = T_{C_\ell} \frac{2R\Delta R\Delta\theta}{R_T^2}$$

$$\Delta P_C = X\, \Delta Q_{C_\ell}$$

3.6 Representation of Airfoil Characteristics

Part of the procedure to analyze the turbine is determining the lift and drag coefficients of the blade element, given the local angle of attack at the blade element. The aerodynamic characteristics of the airfoil section including stall effects must be available to the computer.

It was decided to express the airfoil data as a set of points giving C_L and C_D versus angle of attack. These points are chosen to be at angles of attack at which significant changes in airfoil characteristics occur. Values between these points are found by linear interpolation. Values out of the range of the points input to the computer are found by assuming the lift and drag coefficients degenerate to flat plate values at plus or minus 90 degrees. That is, at 90 degrees, C_L equals zero, and C_D equals 1.2, as shown in Figure 5.

The program is set up to have different airfoil characteristics at different radial positions, thus allowing the user to take into account changes in blade shape and local Reynolds number.

3.7 Centrifugal Effects

The primary centrifugal effect is the change in blade boundary layer due to centrifugal forces near the surface of the blade. W.J. Wentz, Jr., has made some attempt to include three-dimensional stalling effects in the airfoil characteristics (Wentz and Calhoun, 1981)[5]. These studies showed that it is possible that centrifugal effects could double or triple the maximum lift coefficient of the airfoil, with the greatest effect occurring near the hub. When these effects were included in the airfoil characteristics data, the power coefficient was greatly improved at low tip speed ratios. However, the results are currently inconclusive as no data exists to verify these effects.

3.8 Turbulence Effects

Wind turbines are subjected to turbulence covering a wide range of scales. Figure 6 gives the spectrum for horizontal turbulence as a function of the turbulence size at a height of 10 meters (Sachs, 1974)[6]. Note that most of the turbulence occurs at wavelengths around 300 meters. An equation that fits this curve is (Davenport, 1961)[7]

$$\frac{S(n)}{V_0^2}\,dn = 4.0\,K\,\frac{x}{(1+x^2)^{4/3}}\,dx$$

where n is the frequency in cycles per second, S(n) is the spectral density, K is the surface drag coefficient (normalized to the flow velocity at 10 meters), and x, the wave number, is given by

$$x = 1200n/V_0 \quad (V_0 \text{ in m/s})$$

The factor K is typically 0.005 for open, flat terrain. The turbulence intensity, I, in any given size range can be found by integrating this equation over the desired range and taking the square root. Thus,

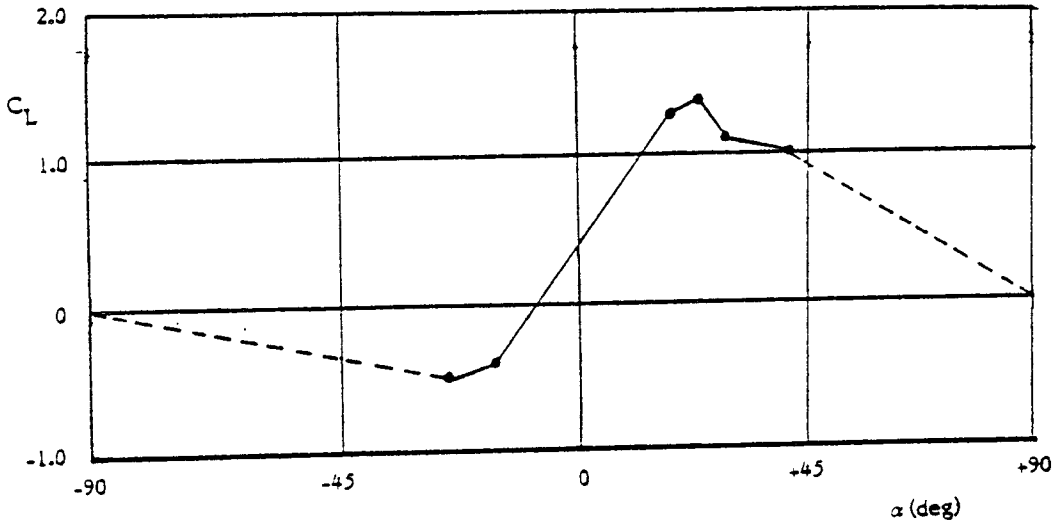

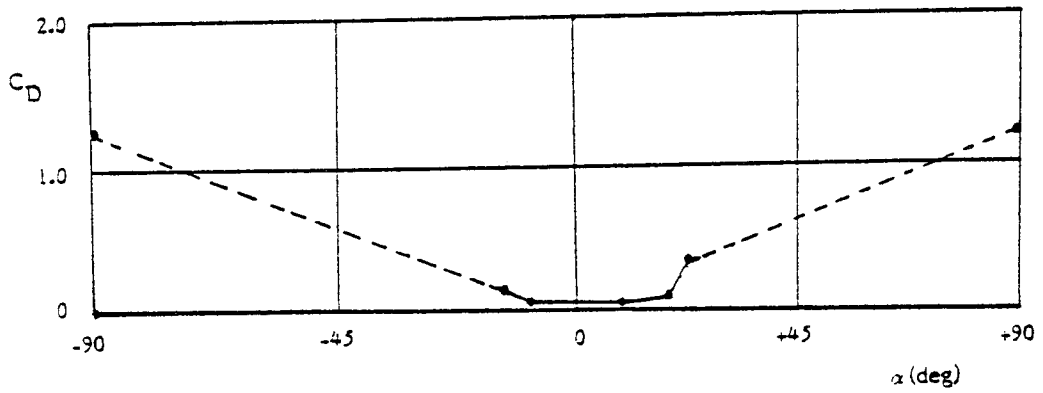

FIGURE 5. Representation of airfoil lift and drag coefficient curves.

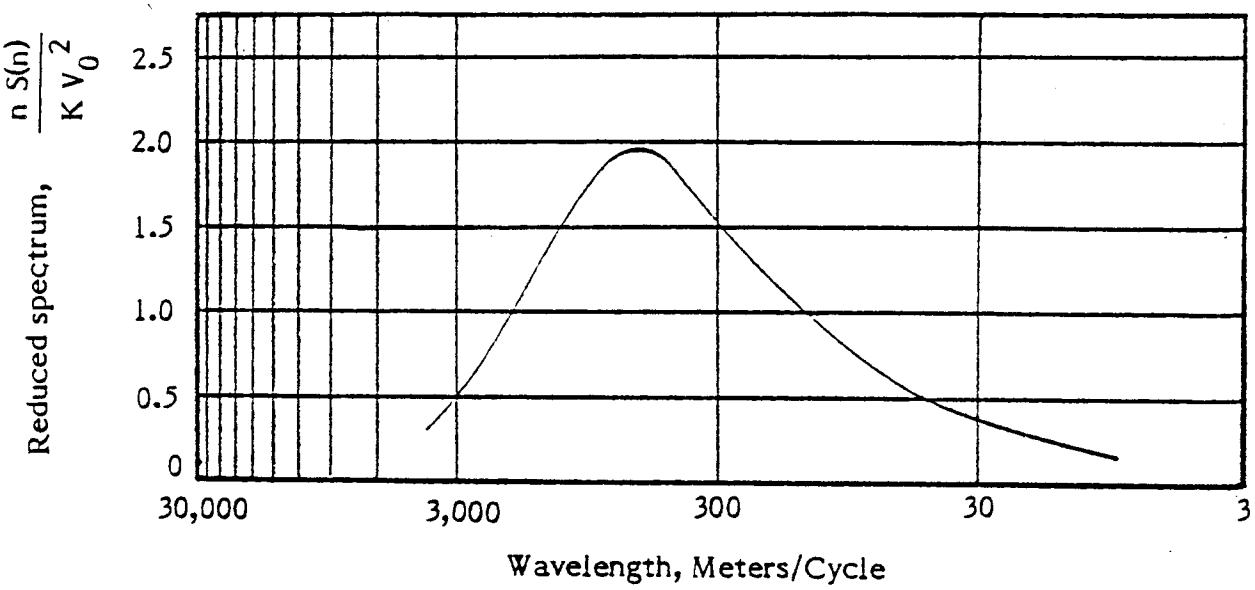

FIGURE 6. Spectrum of horizontal gustiness in high winds, at 10-m height.

$$I = \sqrt{\int_{x_1}^{x_2} S(n)dn/V_0^2}$$

which integrates to:

$$I = 2.45\,K^{1/2} \sqrt{\frac{1}{(1 + x_1^2)^{1/3}} - \frac{1}{(1 + x_2^2)^{1/3}}}$$

Table I gives the turbulence intensity, in percent of V_0, for various turbulence scales in a 10-meter-per-second wind.

Very small scale horizontal turbulence -- that is, turbulence on the same scale as the blade boundary layer depth -- can effect blade element lift and drag characteristics by prematurely tripping the laminar boundary layer. For wind turbines, the level of this turbulence is very low, on the order of 0.57% of the free stream wind. The blades of a modern wind turbine are typically moving 4 to 10 times the speed of the free stream wind, thus making the turbulence level as seen by the blades only 0.14% to 0.057% of the wind speed seen by the blades. This level of turbulence is so low that the section characteristics will be unchanged.

The next scale of horizontal turbulence is in the size range of the rotor radius. Turbulence of this scale can affect part of the rotor blade as the blade cuts through an individual eddy. This can cause angle of attack changes on parts of the blade, thus changing the section lift and drag characteristics. If the angle of attack exceeds the separation angle for the airfoil, it is possible that the section lift coefficient will actually increase above the expected maximum value, maintain that level for a short length of time, and then suddenly stall. This is known as dynamic stall.

The intensity of this scale of turbulence is about 2%. As the blade is typically moving 4 to 10 times faster than the free stream flow, this corresponds to a turbulence of 0.7% to 0.2%, or an angle of attack change of 0.4 to 0.1 degrees. This change is sufficiently small so as to be ignored.

How do you determine $\Delta\alpha$?

The greatest turbulence intensity lies in large scale horizontal turbulence -- that is, turbulence of sufficient size so that the entire turbine is embedded in a constant velocity field over the entire disc. Changes in wind speed can be accounted for by computing the power output of the turbine at all wind speeds, and then doing a time average. This is the realm of capacity factor analysis, not rotor analysis.

Turbulence also causes changes in flow direction. Changes in the horizontal plane are cancelled by the turbine yaw system, provided it is sufficiently responsive. Changes in the vertical plane are not cancelled at all. Vertical turbulence intensity varies with height above the ground but is, in general, less than the horizontal turbulence intensity. Assuming a large value of 13% for vertical turbulence intensity, the corresponding change in flow direction would be 7.5 degrees, which is significant. Thus, it would appear that the only types of turbulence that need be dealt with are the horizontal and vertical components of the large scale turbulence which produce off-axis effects.

TABLE I. Turbulence intensity in a 10 meter per second wind at 10 meters altitude.

Turbulence Scale	Turbulence Intensity	SWECS Turbine Rotor Scale
100 mm and less	0.57%	blade boundary layer
0.1 - 1.0 m	1.4 %	
1.0 - 10.0 m	3.1 %	blade radius
10 - 100 m	6.7 %	
0.1 - 1.0 km	12.8 %	entire turbine
1.0 - 10.0 km	4.7 %	
10 km and greater	1.2 %	
all sizes	17.3 %	

o Off-Axis Flow Effects

The effects of off-axis flow will be examined first by finding the performance of a perfect actuator disc in such flow, and then extending blade element theory to encompass this realm. For a perfect actuator disc placed at an angle to the free stream flow, the flow speed normal to the disc is V_n, and the cross-flow velocity is V_c. As shown in Figure 7, V_c is positive when vertical with θ in the direction of rotation. Both V_c and V_n are normalized by the free stream flow, thus:

$$V_n^2 + V_c^2 = 1.$$

The effect of the disc on the flow is to cause a velocity increment at the disc of magnitude $V_n a$ in a direction normal to the actuator disc. Downstream of the disc, the velocity change will be twice this. The head loss coefficient is

$$C_H = 1 - V_n^2 (1 - 2a)^2 - V_c^2$$

The mass flow coefficient, C_M, is the mass flow through the rotor normalized to the mass flow that would flow through the rotor if V_n is equal to 1 and a is equal to zero.

$$C_M = V_n (1 - a)$$

The power coefficient P_C is

$$P_C = C_H C_M$$

$$P_C = V_n (1 - a) (1 - V_n^2 (1 - 2a)^2 - V_c^2)$$

This expression can be optimized for the best a. Sparing the details, the optimum a is:

$$a = \frac{4V_n - \sqrt{V_n^2 + 3(1 - V_c^2)}}{\sigma V_n}$$

Using the relation $V_n^2 + V_c^2 = 1$, the expression for a can be greatly simplified to $a = 1/3$. Thus, the optimum axial interference factor is not a function of rotor tilt. Using this value for a in the equation for P_C, we obtain

$$P_C = \frac{16}{27} V_n^3$$

Thus, the power coefficient of an ideal actuator disc is proportional to the normal flow velocity cubed, or the cosine of the off-axis angle cubed.

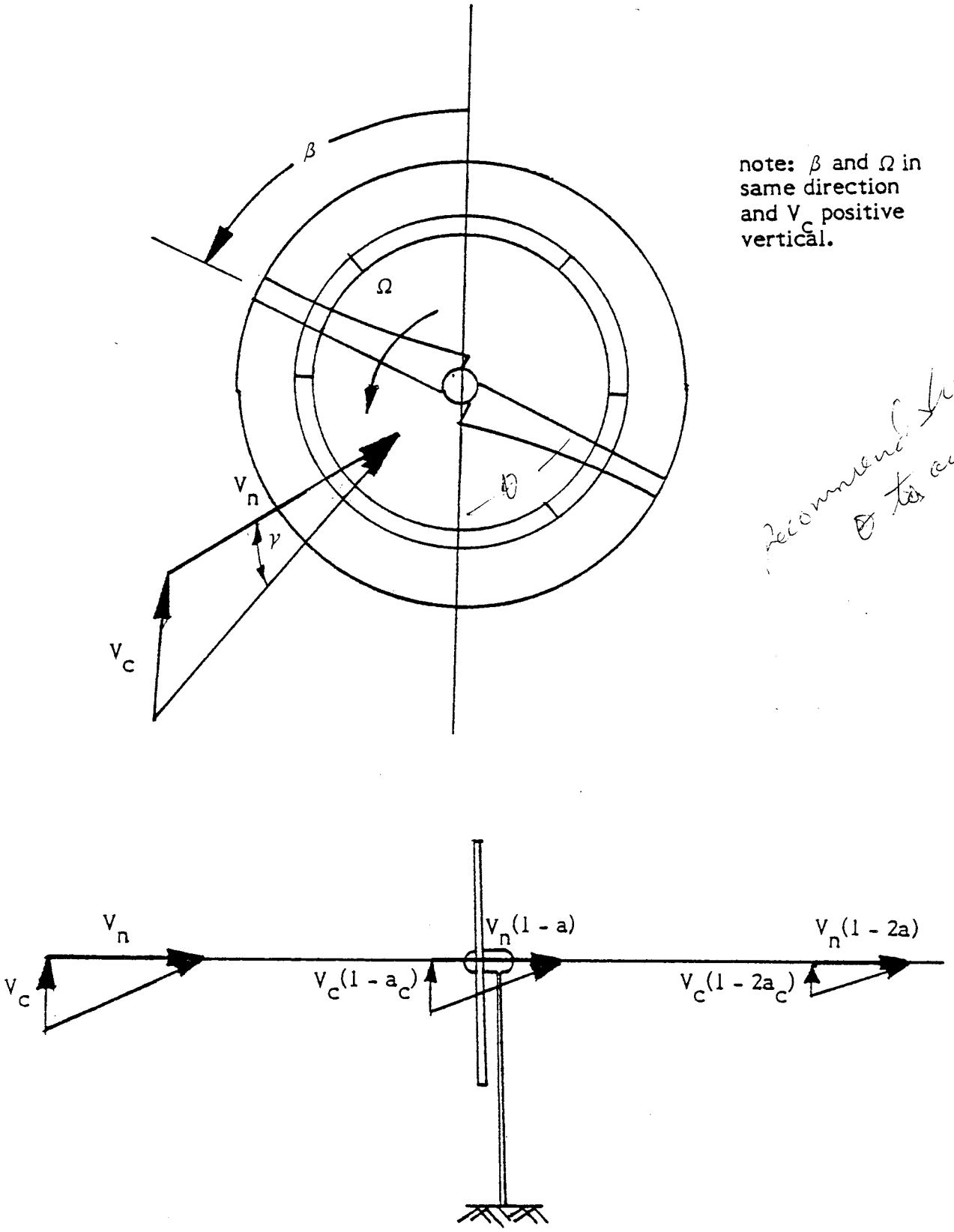

note: β and Ω in same direction and V_c positive vertical.

FIGURE 7. Geometry of cross flow model.

It is also necessary to look at blade element theory when off-axis flow is added. To do this, the blade element force and momentum changes will be resolved into components parallel and perpendicular to the turbine axis. The downstream thrust normal to the plane of rotation is

$$\Delta T = 2\pi R \Delta R \, \rho V_0^2 V_n^2 (1 - a)(2a)$$

for an annulus at radius R, with width ΔR. V_n is the normalized flow velocity normal to the plane of rotation. The cross-flow force is

$$\Delta F_C = 2\pi R \Delta R \, \rho V_0^2 V_n V_c (1 - a)(2a_c)$$

where V_c is the normalized cross-flow velocity, and a_c is the cross-flow interference factor. The total lift generated by the blade element is

$$\Delta L = \tfrac{1}{2} \rho V_0^2 B C \Delta R \left(V_n^2 (1 - a)^2 + (\Omega R + \sin\theta \, V_c (1 - a_c))^2 \right) C_L$$

Defining the incoming flow angle as seen by the blade as φ, the lift force can be resolved into components:

$$\Delta L_N = \Delta L \cos\varphi$$

$$\Delta L_C = \Delta L \sin\varphi \sin\theta$$

Equating the forces in the normal direction we have

$$2\pi R \rho V_0^2 V_n^2 (1 - a)(2a) \Delta R = \tfrac{1}{2} \rho C B \, \Delta R \, V_0^2 \left(V_n^2 (1 - a)^2 + \right.$$

$$\left. (\Omega R + \sin\theta \, V_c (1 - a_c))^2 \right) C_L \cos\varphi$$

or

$$(1 - a)(2a) = \frac{1}{2} \frac{CB}{2\pi R} \left((1 - a)^2 + \left(X_n + \sin\theta \frac{V_c}{V_n} (1 - a_c) \right)^2 \right) C_L \cos\varphi$$

where $X_n = X/V_n$.

Using the relation,

$$W^2 = (1 - a)^2 + \left(X_n + \sin\theta \frac{V_c}{V_n} (1 - a_c) \right)^2$$

or

$$W^2 = (1 - a)^2/\sin^2\varphi$$

where

$$\varphi = \text{atan}\left[(1 - a)/(X_n + \sin\theta \frac{V_c}{V_n}(1 - a_c))\right]$$

we can simplify the relation to:

$$(1 - a)(2a) = \frac{1}{2} \frac{CB}{2\pi R} \frac{(1 - a)^2 C_L \cos\varphi}{\sin^2\varphi}$$

Equating the cross-forces we have:

$$2\pi R \rho V_0^2 V_n V_c (1 - a)(2a_c) \Delta R = \frac{1}{2}\rho C \Delta R B V_0^2 \Big(V_n^2 (1 - a)^2$$

$$+ (\Omega R + \sin\theta V_c (1 - a_c))^2\Big) C_L \sin\theta \sin\varphi$$

or

$$(1 - a) 2a_c = \frac{1}{2} \frac{CB}{2\pi R} \frac{V_n}{V_c} \left((1 - a)^2 + (X_n + \sin\theta \frac{V_c}{V_n}(1 - a_c))^2\right) C_L \sin\theta \sin\varphi$$

and substituting in the relation for W,

$$(1 - a) 2a_c = \frac{1}{2} \frac{CB}{2\pi R} \frac{V_n}{V_c} \frac{C_L \sin\theta}{\sin\varphi}$$

These equations were solved for a and a_c for some test examples. They were not incorporated into the main computer model. It should be noted that in deriving these relations, circumferential interference and tip loss have been ignored.

The first test case was for a two-bladed turbine with a C/R of 0.075, no twist, no feather, and with the blade element of interest moving at a tip speed ratio of 7. This is close to optimum operating conditions.

Figure 8 shows the local torque coefficient, Q_C, as a function of blade position for zero, 10, and 20 degrees off-axis flow. Also given are the average values for Q_C for this one annulus, and a comparison to the cosine cubed law. As can be seen, the comparison is good.

Figure 9 shows the results for the same blade element, but at a feather angle of five degrees. This is an off-optimum condition. The comparison with the cosine cubed law is still good.

don't clear who this case includes, relate to following for a and a_c. Interesting info but somehow you need to tie it to the introduction through

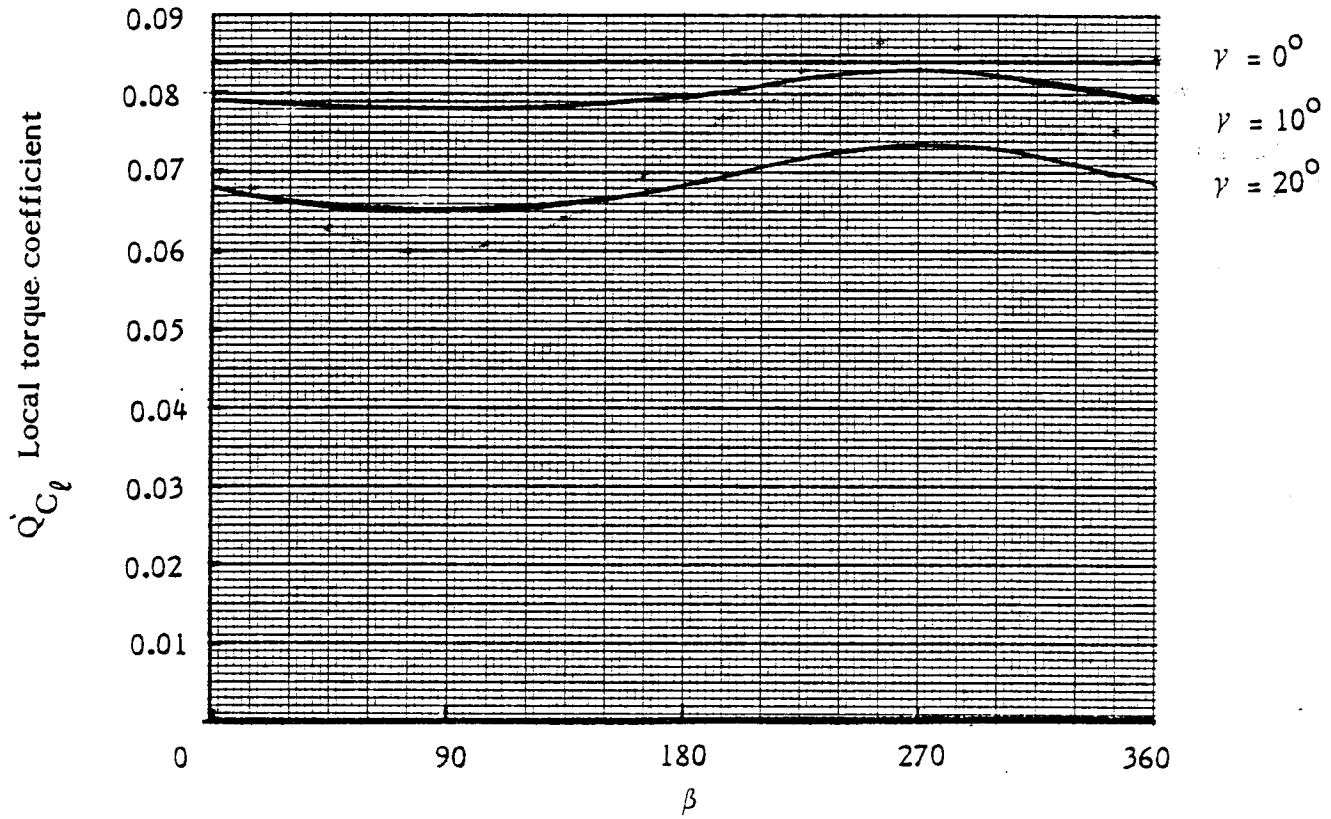

Inflow angle, γ	Average Q_{C_ℓ}	Q_{C_ℓ} ($\gamma = 0$) x $\cos^3 \gamma$
0	0.0842	0.0842
10	0.0802	0.0804
20	0.0688	0.0699

FIGURE 8. Torque coefficient of a blade element with a chord of 0.075, two blades, zero feather angle, at a speed ratio of 7.

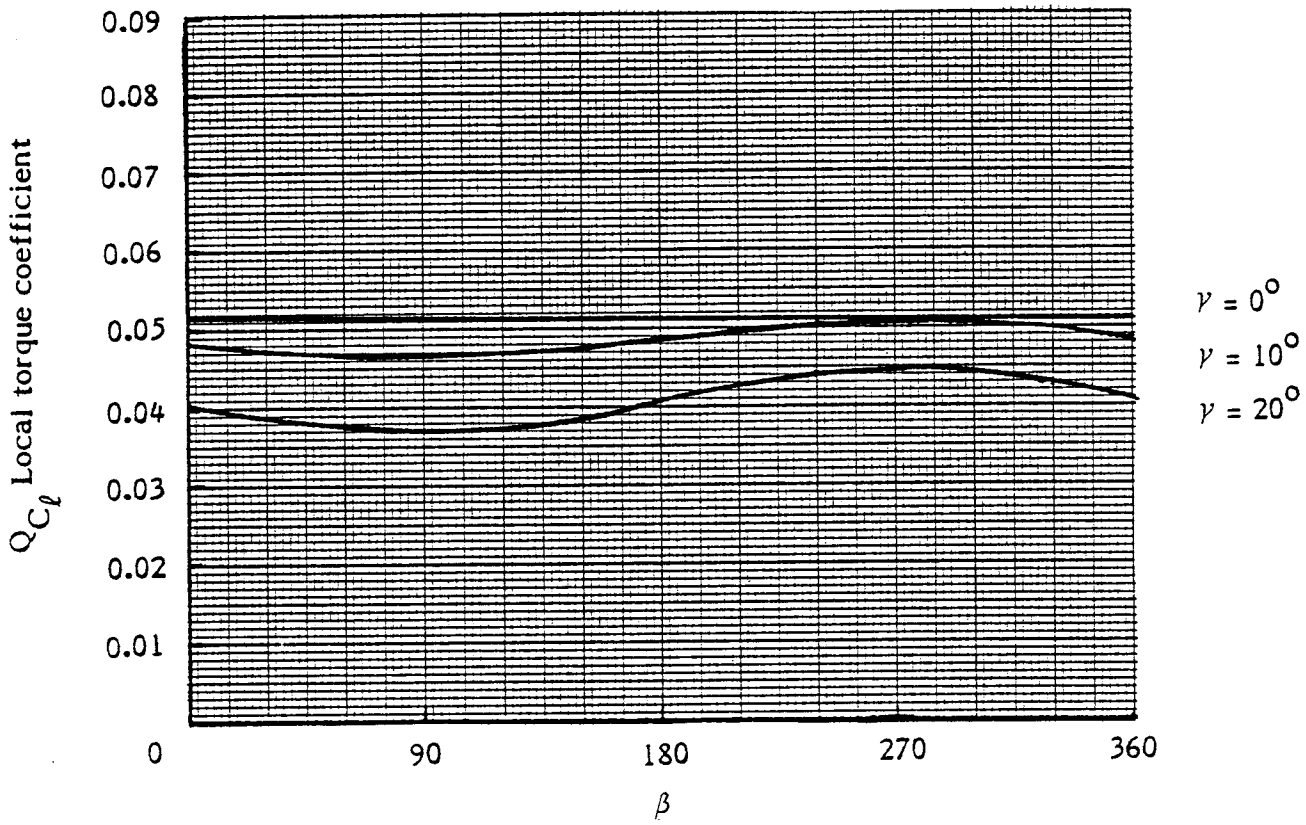

Inflow angle, γ	Average Q_{C_ℓ}	$Q_{C_\ell}(\gamma = 0) \times \cos^3 \gamma$
0	0.0517	0.0517
10	0.0488	0.0494
20	0.0407	0.0429

FIGURE 9. Torque coefficient of a blade element with a chord of 0.15, 5 degrees pitch angle, at a tip speed ratio of 7.

The conclusion from this is that the turbine will respond only to the normal component of the flow, and ignore any cross-flow. Thus, if a 13% turbulence is assumed, the axial flow will be reduced to 99.2% of its full value, resulting in a 2.5% power loss.

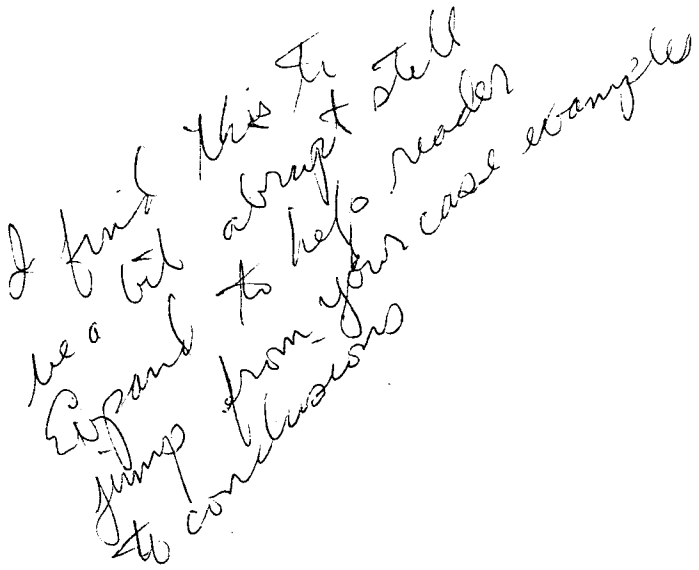

4.0 INPUT/OUTPUT PARAMETERS FOR THE COMPUTER MODEL

The computer program requires the following input parameters, and produces the following results:

- o Input

  Rotor geometry:

  Number of blades.
  Cone angle (degrees).
  Hub cut out radius (normalized).
  Tip and hub loss models (Prandtl, or none).
  Brake state model (classical or advanced).
  Wind shear exponent, hub height (normalized), and number of circumferential stations.

  Blade element data (blade is divided into ten equal segments):

  Note: All quantities are measured at the mid-point of the elements

  Chord (normalized), and twist of each of the ten blade elements.
  Airfoil section lift coefficient versus angle of attack, and drag coefficient versus angle of attack for each blade element.

  Analysis ranges:

  Feather angle range and increment.
  Advance ratio range and increment.
  Blade elements to include in analysis (this is to allow examination of only part of the rotor for design optimization purposes).

- o Output

  Blade element data:

  For each feather angle, advance ratio, circumferential station, and blade element, the values for $\underline{a}$, a', C_L, C_D, φ, angle of attack (α), and the torque, thrust, and power coefficients normalized to the annulus area, are output.

  Complete rotor data:

  For each feather angle and advance ratio, the total values for the torque, thrust, and power coefficients are output.

In the current form of the program, outputing of the blade element data is optional.

5.0 SPECIFIC TURBINE ANALYSIS AND RESULTS

For this project, two turbines specified by the sponsor were analyzed using three different options of the model. The options used were the classical brake state model with no wind shear, advanced brake state model with no wind shear, and advanced brake state with a 0.167 wind shear exponent. The runs with wind shear used four circumferential stations.

For machine A, the rotor was analyzed at feather angles of -4°, 0°, 4°, and 8°. The tip speed ratio was varied from 0.5 to 12.0 in steps of 0.5. The airfoil section data used was obtained directly from data supplied by the sponsor. The blade Reynolds number was derived from the blade geometry and the operating RPM of 170. This resulted in the use of NACA 4415 data at $Re = 83 \times 10^3$ for sections 1 through 3, NACA 4415 data at $Re = 163 \times 10^3$ for sections 4 through 6, NACA 4415 data at $Re = 334 \times 10^3$ for sections 7 through 9, and NACA 4412 data at $Re = 334 \times 10^3$ for the outer section, 10 .

For machine B, the rotor was analyzed for feather angles of -2°, 0°, and 2°. The tip speed ratio was varied from 1.0 to 15.0 in steps of 0.5. The airfoil section characteristics were taken from the NACA 0012 data provided, using the $Re = 170 \times 10^3$ data for sections 1 to 6, and the $Re = 330 \times 10^3$ data for sections 7 through 10.

Computer output from these analyses is presented in Appendix A. For each run, the input parameters are listed, the rotor performance given, and a plot of P_C versus X for the feather angles considered are given. The element data is not output as this would add about 200 pages of output.

In examining the results of the analysis of the two rotors (data presented in Appendix A), a number of interesting conclusions can be drawn. Rotor A has a maximum P_C of 0.397 at design feather angle and a tip speed ratio of 5.0 to 5.5. However, at a feather angle of 4°, the maximum power coefficient is 0.442 at a tip speed ratio of 6.0. Examination of the power coefficient curves reveal that performance is better at almost all tip speed ratios at this feather angle.

Rotor B has a maximum P_C of 0.337 at design feather angle and tip speed ratios of 8.0 to 8.5. Off-design feather angles result in lower performance.

For both rotors it would appear that adding wind shear makes almost no difference in performance. In fact, test cases have shown that even rotors as near to the ground as a MOD-2 rotor have only a three-percent performance loss due to wind shear. The rotors under consideration have hub heights so great (normalized to rotor radius) that the wind speed variation is very small, resulting in the nearly insignificant performance change.

The effects of which brake state model is used are more dramatic. At low tip speed ratios, there is no difference in the results, as the rotor is not in the brake state. The changes in predicted results occur at high advance ratios and/or negative feather angles. The advanced brake state model gives higher power coefficients at these points than the classical model. The curves given by the classical model tend to have an abrupt performance drop when the rotor enters the brake state. The advanced model tends to give smoother curves. Because the advanced model is based on observed data, it is felt that it will give performance predictions closer to the experimental results.

6.0 COMPARISON OF THEORY AND EXPERIMENT

Performance data for the two turbines analyzed in Chapter 5 were given to AV by Rockwell International. The two turbines were tested by Rockwell using a turbine mounted on a moving flatcar at the U.S. Department of Transportation's test center at Pueblo, Colorado. The tests were made at a constant RPM with various tip speed ratios obtained by changing the speed of the train on which the turbine was mounted. System performance was determined by measuring the electrical power output of the generator. Corrections were then applied for power train efficiency, density, and off-axis flow to estimate rotor performance. The correction made for off-axis flow was a cosine to the first power correction, not the cosine cubed correction advocated by AV. Rockwell suggested that the cosine correction is better supported by data, so the Rockwell correction was used.

In this chapter, experimental data are compared to the theoretical curves, discrepancies between theory and experiment are investigated, an improvement is made in the treatment of airfoil characteristics in the stall range, and the data are compared to the improved theoretical curves. Section 6.1 discusses the comparison of the data with the original performance predictions, and Section 6.2 discusses improvements to the theoretical model, and comparison of the data with the improved model.

6.1 Comparison of Data With the Original Prediction

For each turbine, performance predictions were made for three cases: (1) classical brake state model, (2) advanced brake state model, and (3) advanced brake state model with wind shear. Case 3 is of little significance, as it is almost indistinguishable from the no-wind shear case, and the test data was generated in no-shear conditions. On the basis of the test data, it cannot be determined which of the two brake state models is best, as the test data was only reported for tip speed ratios below the tip speed ratios for which brake state was predicted to begin. The advanced model is still preferred, however, as it gives smoother performance curves. Thus, the data will be compared to the advanced brake state model/no-wind shear prediction.

Data for the Enertech 1500 rotor (machine A) is compared to theory in Figure 10. Comparison is good, with the worst error being on the order of 0.04 in power coefficient at a tip speed of 5. The maximum predicted power coefficient is 0.397, compared to 0.37 for the data. For tip speeds less than 4, the comparison is excellent. The discrepancies at higher tip speeds may be due to errors in the airfoil data used. The prediction was made assuming NACA 4412 and 4415 airfoil data. In actuality, the Enertech rotor does not use this airfoil, but one similar to it. Actual airfoil data for the Enertech rotor sections would be needed to make a proper evaluation. It is noted that increasing the blade twist angle by 4^{o} results, theoretically, in higher performance. In general, the comparison of theory and data is quite good.

Figure 11 shows the data and theory for the one-third scale UTRC turbine (Machine B). The curves do not agree well. The discrepancy between the two curves is greatest at a tip speed of 8, where theory gives a power coefficient of 0.32, but data gives only 0.21. This large difference can be accounted for by assuming a large, unidentified source of drag for the turbine blades. If a C_D increment of 0.020 is assumed along the entire blade span at

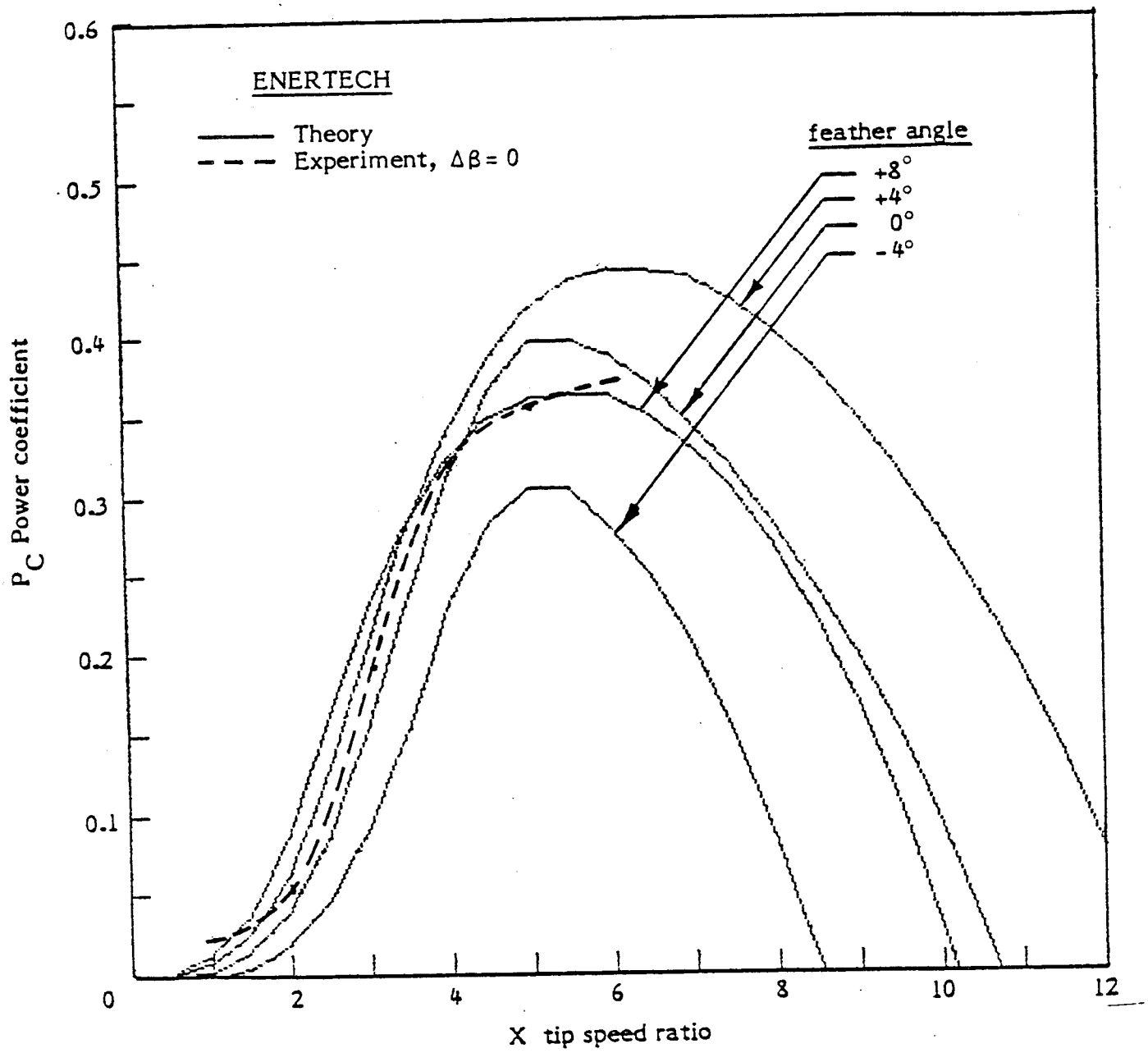

FIGURE 10. Enertech turbine comparison, original prediction.

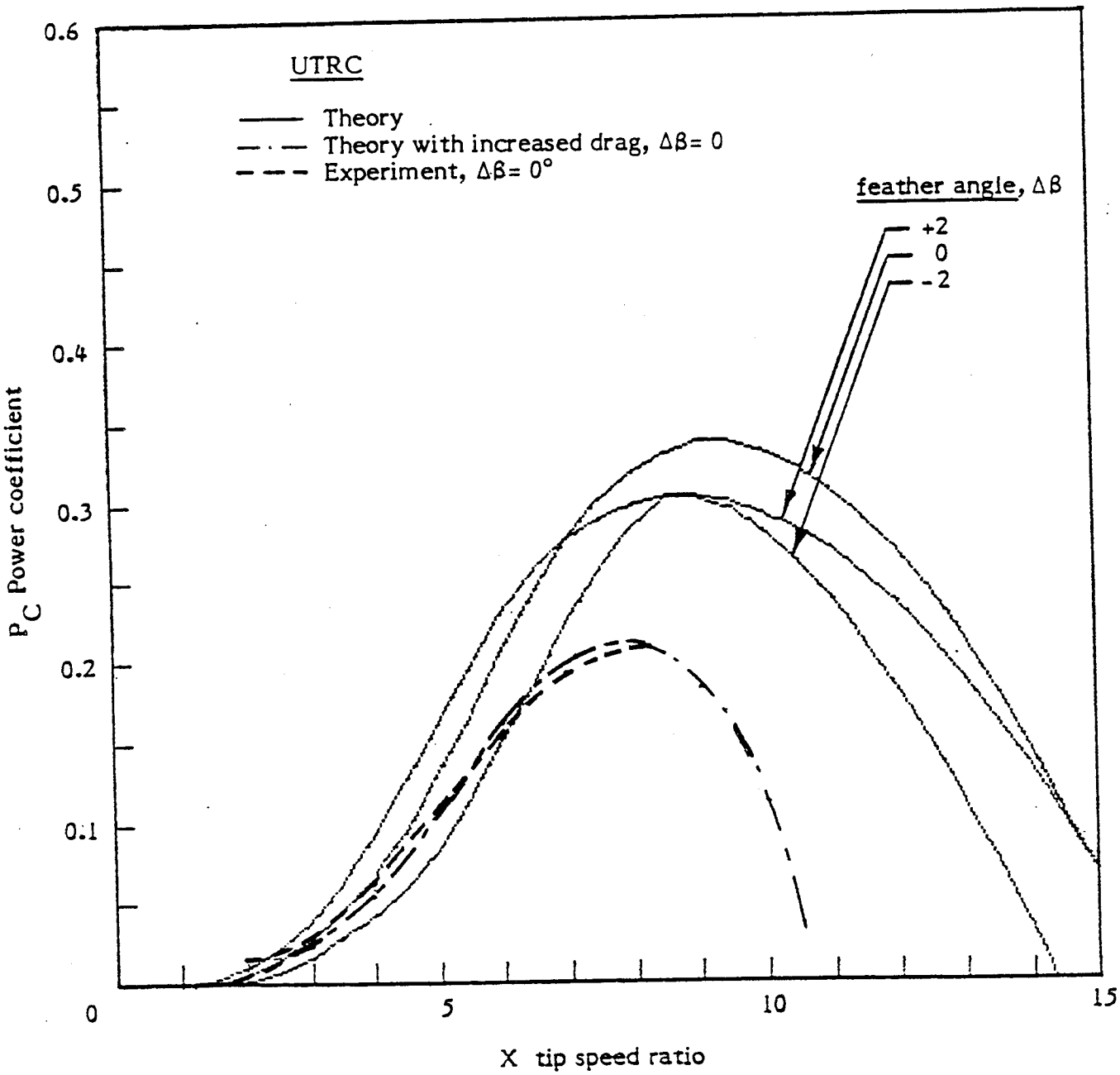

FIGURE 11. UTRC turbine comparison, original prediction.

all angles of attack, then the performance is as shown in the lower curve in Figure 11, and here agreement is good. An increase in section drag coefficient of 0.020 is quite large, as it more than doubles the drag. This increase cannot be explained as a low Reynolds number effect because the airfoil data originally used was low Reynolds number data. Premature stall is not a possibility as the performance loss occurs at high tip speed ratios where the airfoil will not be stalled. The most likely drag source is due to the improper construction of the airfoil section or, as suggested by Rockwell personnel, there may have been aeroelastic deformation of the model under test. Checking the theoretical model against data for the full-scale UTRC turbine would help clear up the problem.

It is believed that the one-third scale UTRC model gave such poor performance, with a maximum power coefficient of 0.21, that there had to be some source of high rotor drag not identified in the test program.

6.2 Modifications to the Theoretical Model

With the proper selection of airfoil characteristics, it has been shown that the theory and data agree well. However, the airfoil characteristics used by the model for the stalled region are somewhat arbitrary; the lift coefficient is decreased linearly to zero at an angle of attack of 90°, and the drag coefficient is increased linearly to 1.2 at 90°. A better description of the stalled airfoil characteristics was developed to enable better performance prediction at low tip speed ratios (corresponding to high wind speeds in constant RPM systems, an area where airfoil stall is used to control power output) and starting torque.

Would be helpful to explain why this is so.

o Approach

To illustrate the problem with the original assumptions in the stall region, the airfoil characteristics used in the analysis of the Enertech and UTRC rotors are shown in Figure 12. The lift and drag components can be resolved into forces normal and tangential to the airfoil chord line, with the tangential coefficient (C_t) shown. In the deep stall region, above about 25° to 30°, the C_t value should be zero, the airfoil being subject to normal forces only in a manner similar to a flat plate. The characteristics used do not give this result. To improve the treatment in the stalled region, a stalled flat plate model was developed using analytic expressions for C_L and C_D. As will be shown, this model did not result in acceptable predictions for the two rotors. The reason for this was found to be that the airfoil characteristics between 12° and 26° degrees, the shallow stall range, did not agree well with the available data.

To remedy this situation, an empirical modification was made to the stalled flat plate model characteristics in the shallow stall range of angles of attack, 12° to 26°. The resulting modified stalled flat plate model showed much better agreement with the experimental data for the Enertech and UTRC rotors and has been included in the final version of the model.

Both the stalled-flat-plate and modified-stalled-flat-plate models are discussed in the following subsections.

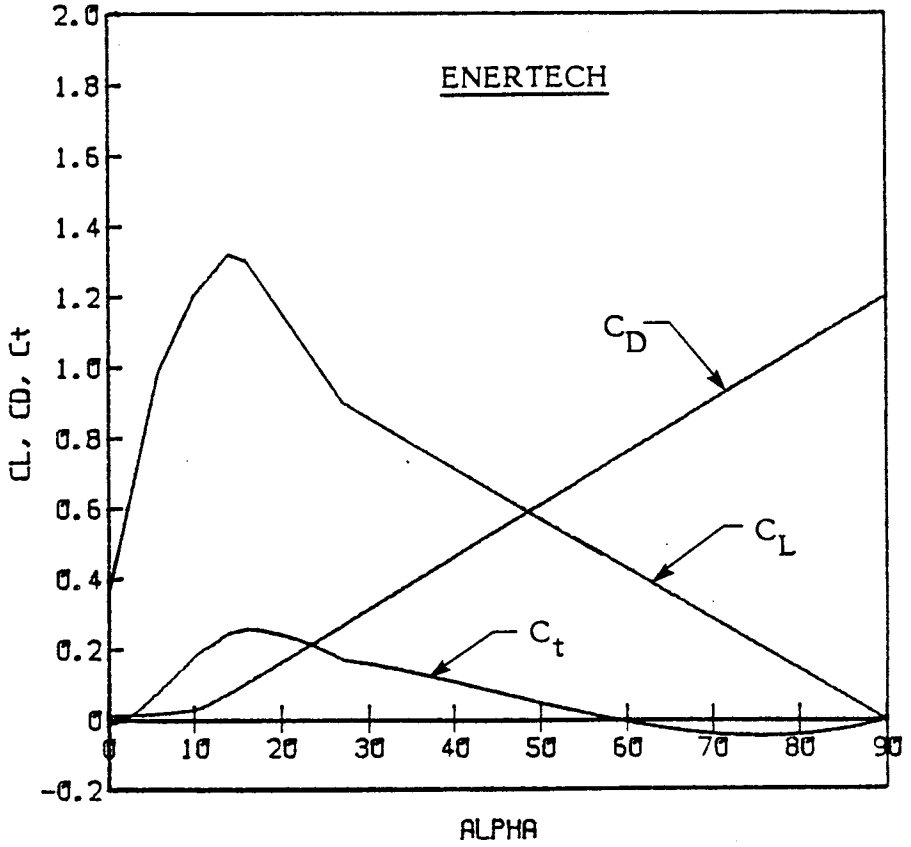

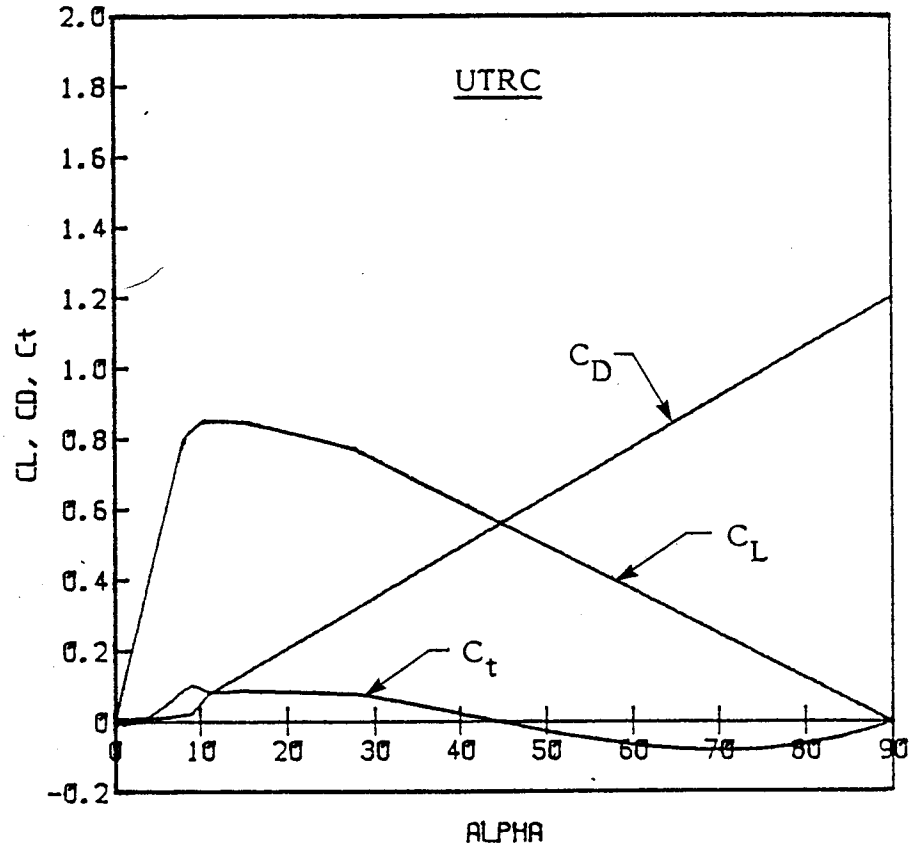

FIGURE 12. Airfoil characteristics used in the original prediction.

o Stalled-Flat-Plate Model

Forces on a stalled flat plate have been examined by Horner (1965)[8]. The normal force coefficient, C_n for a low aspect ratio (less than 5) flat plate is 1.17 for angles of attack greater than about 25^o. For two-dimensional flat plates, C_n is

$$C_n = \frac{1}{0.222 + 0.283/\sin\alpha}$$

At an angle of attack of 90^o, C_n is given for various blade aspect ratios (AR) as

$$C_n = 1.98 - 0.81 \tanh\left(\frac{12.22}{AR}\right)$$

Figure 13 shows the normal force coefficient for flat plates at various angles and aspect ratios. From this, it can be seen that C_n can be expressed as follows:

$$C_n = \min\left(\frac{1}{0.222 + 0.283/\sin\alpha}, 1.98 - 0.81 \tanh\left(\frac{12.22}{AR}\right)\right),$$

where "min" refers to the minimum function; i.e., the lowest of the two possibilities. Once C_n is known, C_L and C_D can be found directly

$$C_L = C_n \cos\alpha, \quad \text{and} \quad C_D = C_n \sin\alpha .$$

It is still necessary to determine the aspect ratio of an element of turbine blade. The apparent aspect ratio can be related to the Prandtl tip loss factor, F. One interpretation of the tip loss factor is that it is the amount of lift lost; that is,

$$F = \frac{C_L}{C_{L_o}},$$

where C_L is the actual lift coefficient, and C_{L_o} is the lift coefficient that would be obtained if there was no tip loss. A similar relationship holds for finite aspect ratio blades,

$$\frac{a}{a_o} \approx \frac{1}{1 + 2/AR} = \frac{C_L}{C_{L_o}} .$$

Equating these two relationships,

$$F = \frac{1}{1 + 2/AR},$$

and solving for the aspect ratio,

$$AR = \frac{2F}{1 - F},$$

gives an equation for an apparent aspect ratio as a function of F.

The flat plate model is integrated with the airfoil characteristics as follows. Standard airfoil test data is used until stall occurs. The C_L and C_D curves are then linearly

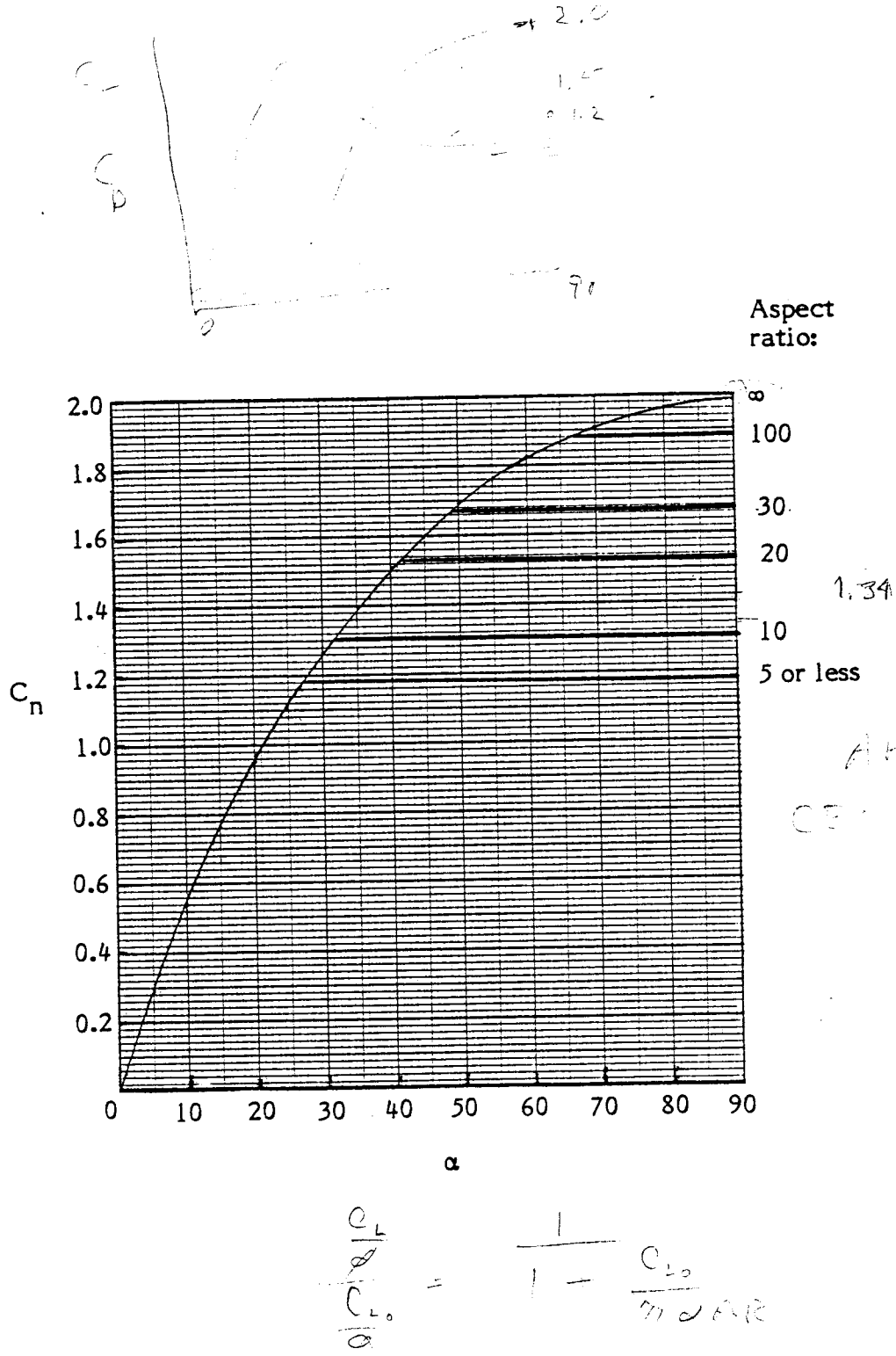

$$\frac{\frac{C_L}{\alpha}}{\frac{C_{L_0}}{\alpha}} = \frac{1}{1 - \frac{C_{L_0}}{\pi \alpha AR}}$$

FIGURE 13. Normal force coefficient on a stalled flat plate of finite aspect ratio.

$$\alpha = \frac{\alpha_0}{1 + \frac{\alpha_0}{\pi AR}}$$

$$\frac{\alpha}{\alpha_0} = \frac{1}{1 + \frac{\alpha_0}{\pi AR}}$$

extended from the last data point just after stall to the flat plate stall values at $\alpha = 26.5^{\circ}$, where $C_L = 1.047$ and $C_D = 0.522$. The angle 26.5° is used because it is the greatest angle of attack for which the flat plate C_n is not a function of aspect ratio.

Figure 14 shows the resulting stalled-flat-plate-model airfoil characteristics. These curves were compared with wind tunnel data for the 0012 airfoil operated at high angles of attack (Critzos et al., 1955)[9] and were found to agree well. Figures 15 and 16 show the performance prediction based on these characteristics for the Enertech and for the UTRC rotors, respectively. In both cases, the performance is underpredicted in the mid to low tip speed range. An examination of the polars reveals the reason: C_t has been greatly reduced in the shallow stall (less than $\alpha = 26.5^{\circ}$) region.

o Modified-Stalled-Flat-Plate Model

In the shallow stall region, the flow is still partially attached to the upper surface of the airfoil. Thus, drag should be less than the flat plate case, and the lift should be greater. An examination of stalled-flat-plate model airfoil characteristic curves shows that the lift is indeed greater, but the drag is about the same as the stalled flat plate. Thus, to properly model the airfoil, the drag should be reduced. An empirical drag curve was developed which resulted in good predictions for both rotors. This curve was generated by increasing the C_D at a rate of 0.019 per degree from the stall angle to 20°, and then letting C_D increase linearly to 0.522 at 26.5°. From this point onward the flat plate model is used.

Figure 17 shows the modified-stalled-flat-plate airfoil characteristics for the Enertech and UTRC airfoils. Figure 18 shows the performance prediction for the Enertech rotor, and Figure 19 shows the prediction for the UTRC rotor. The computer output of the performance prediction is given in Appendix A. Agreement with the data is good. It should be noted that this modification to the drag curve is empirical and, as yet, not supported by theory. However, the drag of an airfoil section normally increases quadratically in the shallow stall region, not linearly as originally assumed. The shallow stall model used is an approximation to a quadratic drag increase. More research is needed to determine the proper airfoil characteristics in this regime.

It is also possible that the centrifugal effects discussed in Section 3.7 may be responsible for the remaining discrepancy between theory and the data. Again, more research is needed.

Here again, it is noted that this modified-stalled-flat-plate model for airfoil characteristics has been chosen as the best approach and has been incorporated in the final version of the computer program.

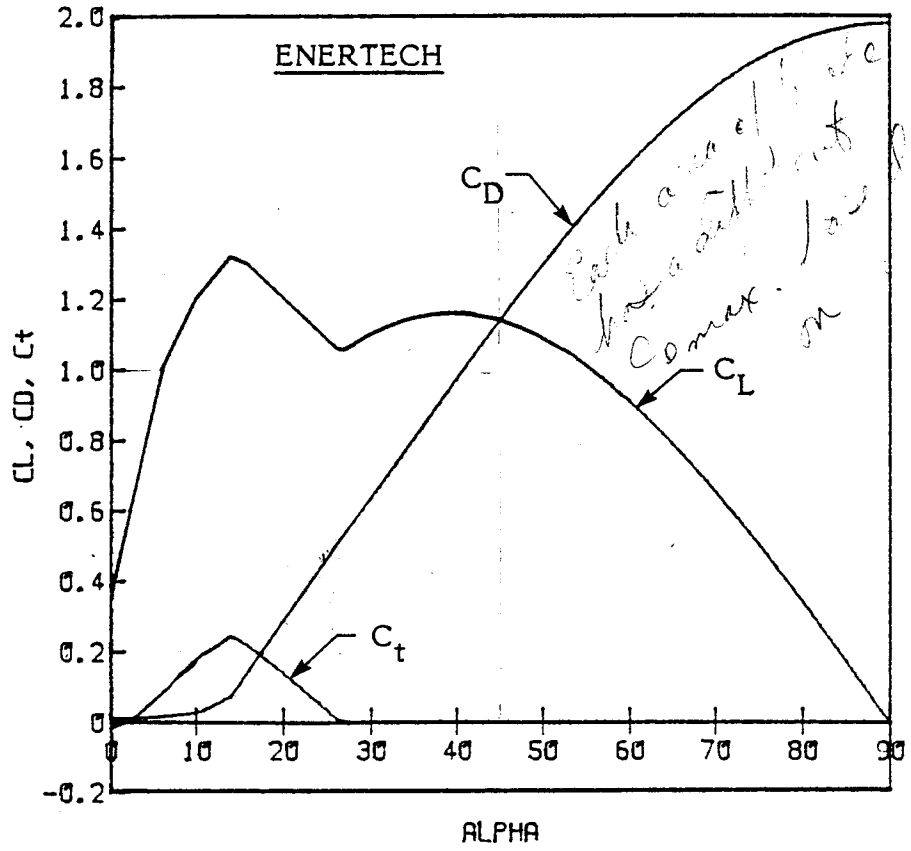

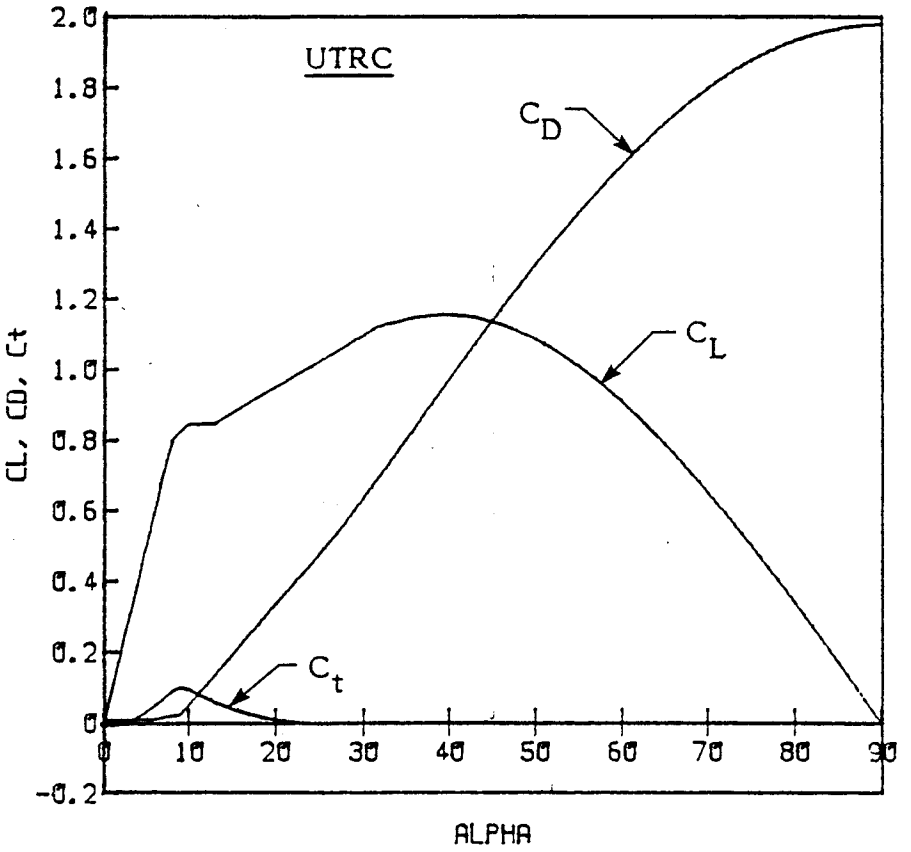

FIGURE 14. Airfoil characteristics, stalled flat plate model.

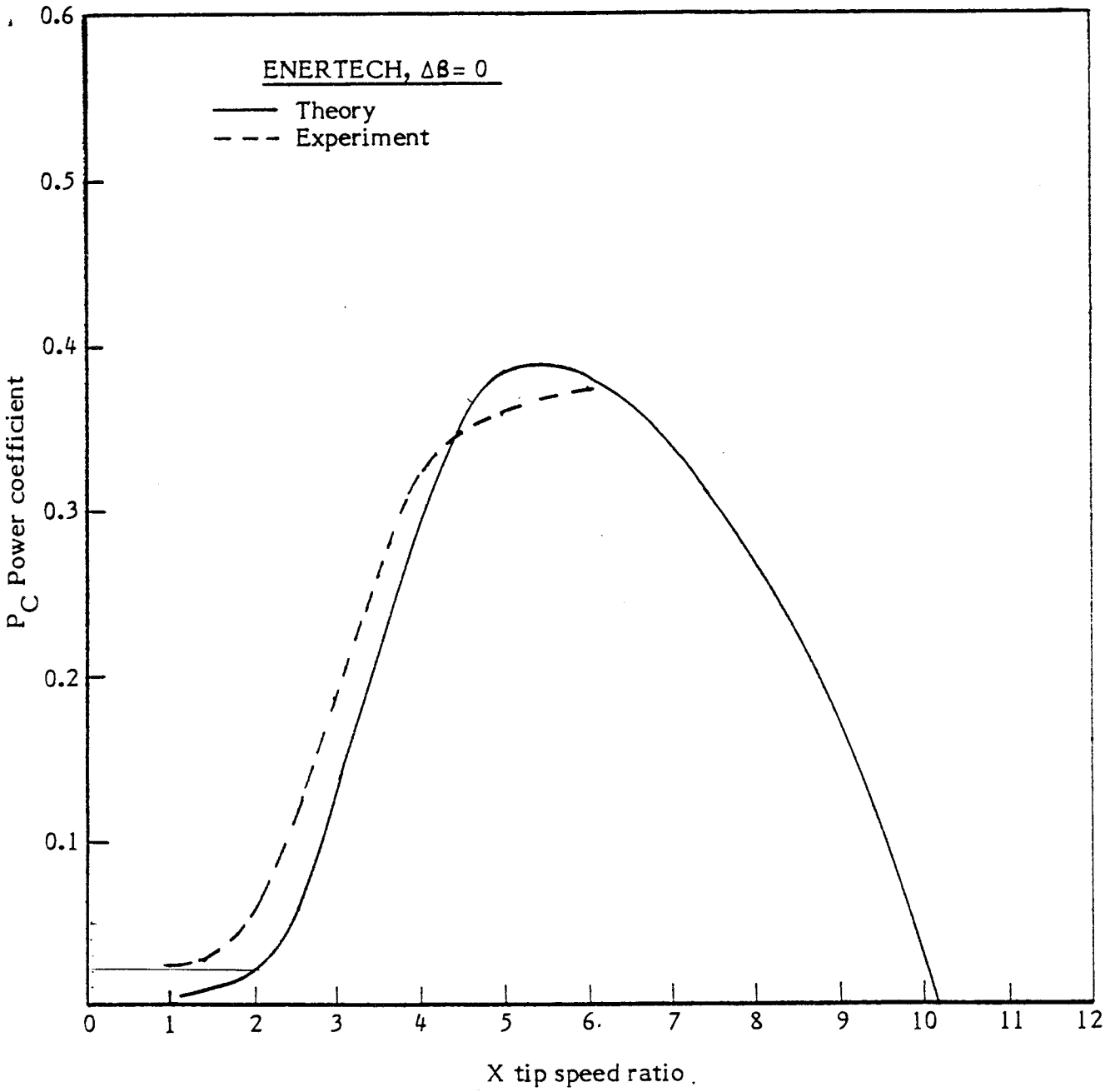

FIGURE 15. Enertech turbine comparison with theory, stalled flat plate model used, $\Delta\beta = 0°$.

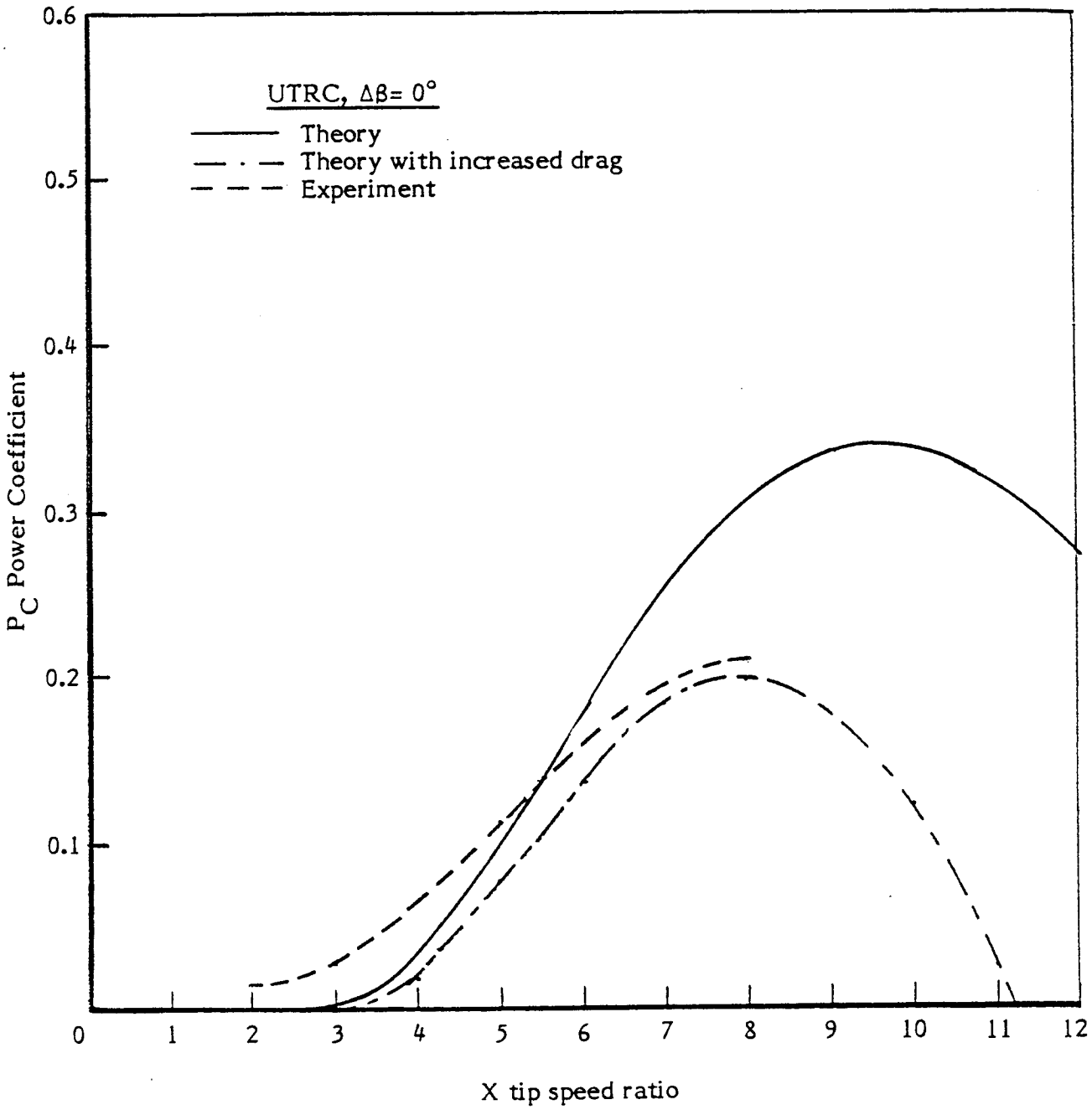

FIGURE 16. UTRC turbine comparison with theory, stalled flat plate model used, $\Delta\beta = 0^{o}$

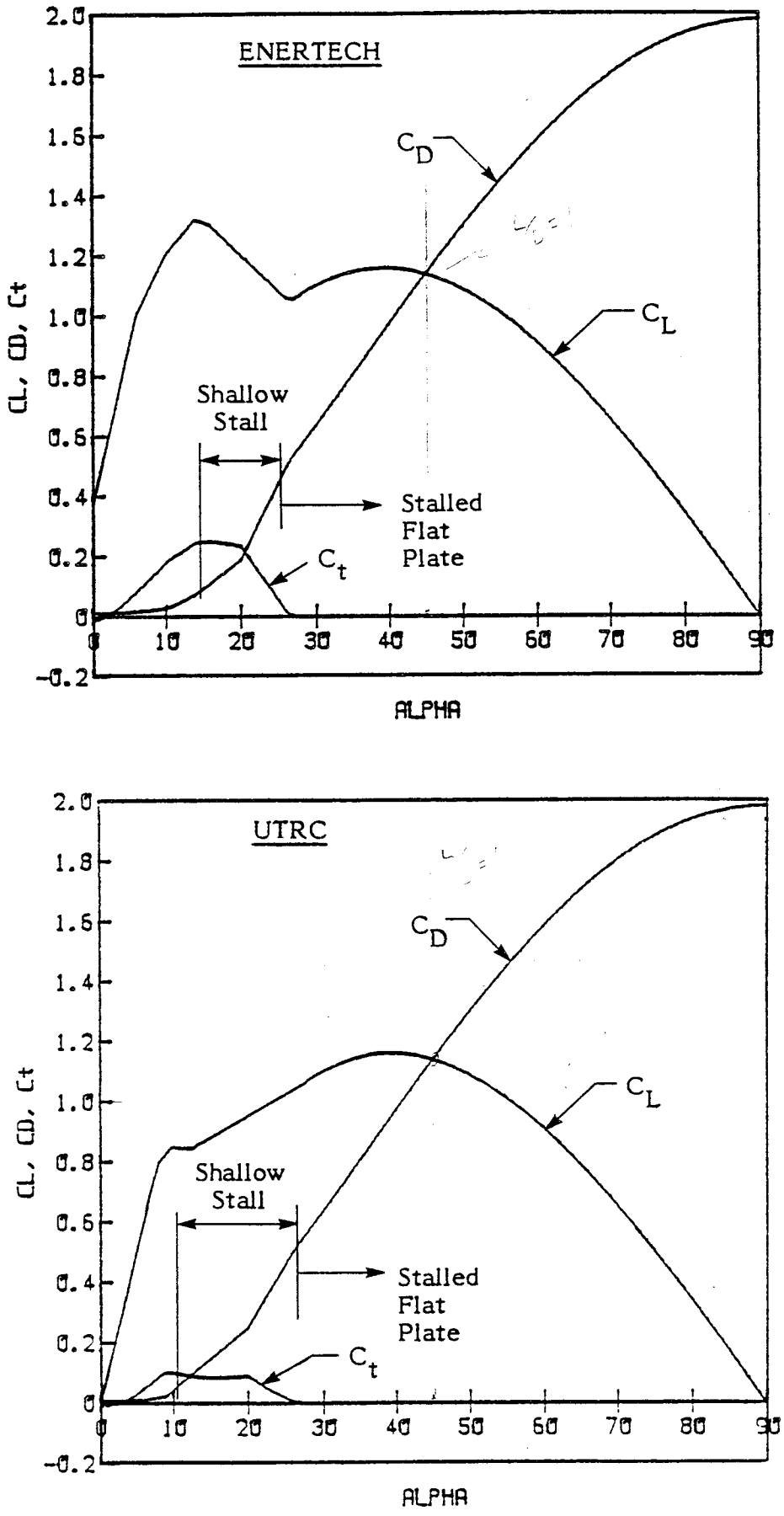

FIGURE 17. Airfoil characteristics, modified stalled flat-plate model.

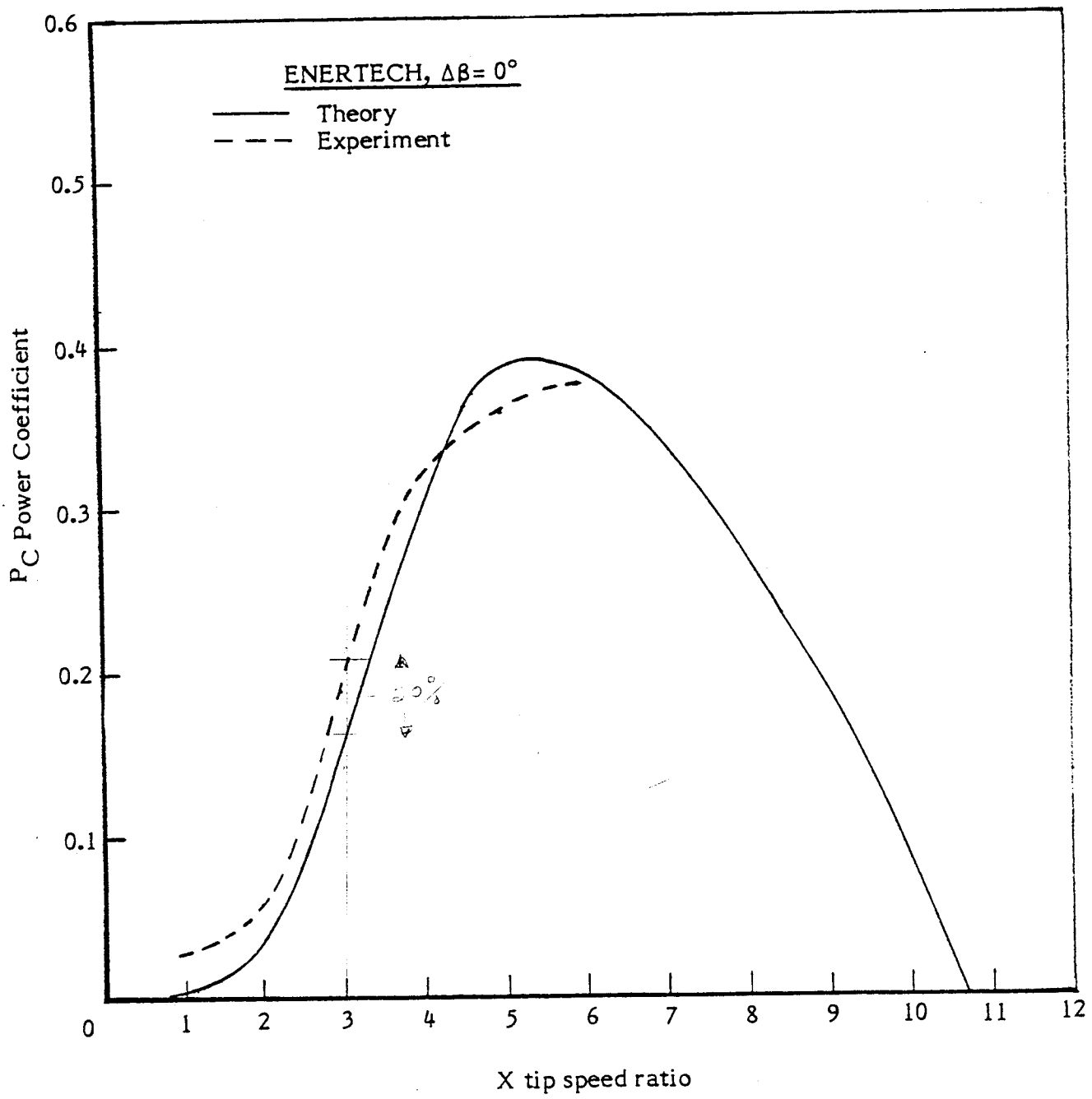

FIGURE 18. Enertech turbine comparison to theory, modified stalled flat-plate model.

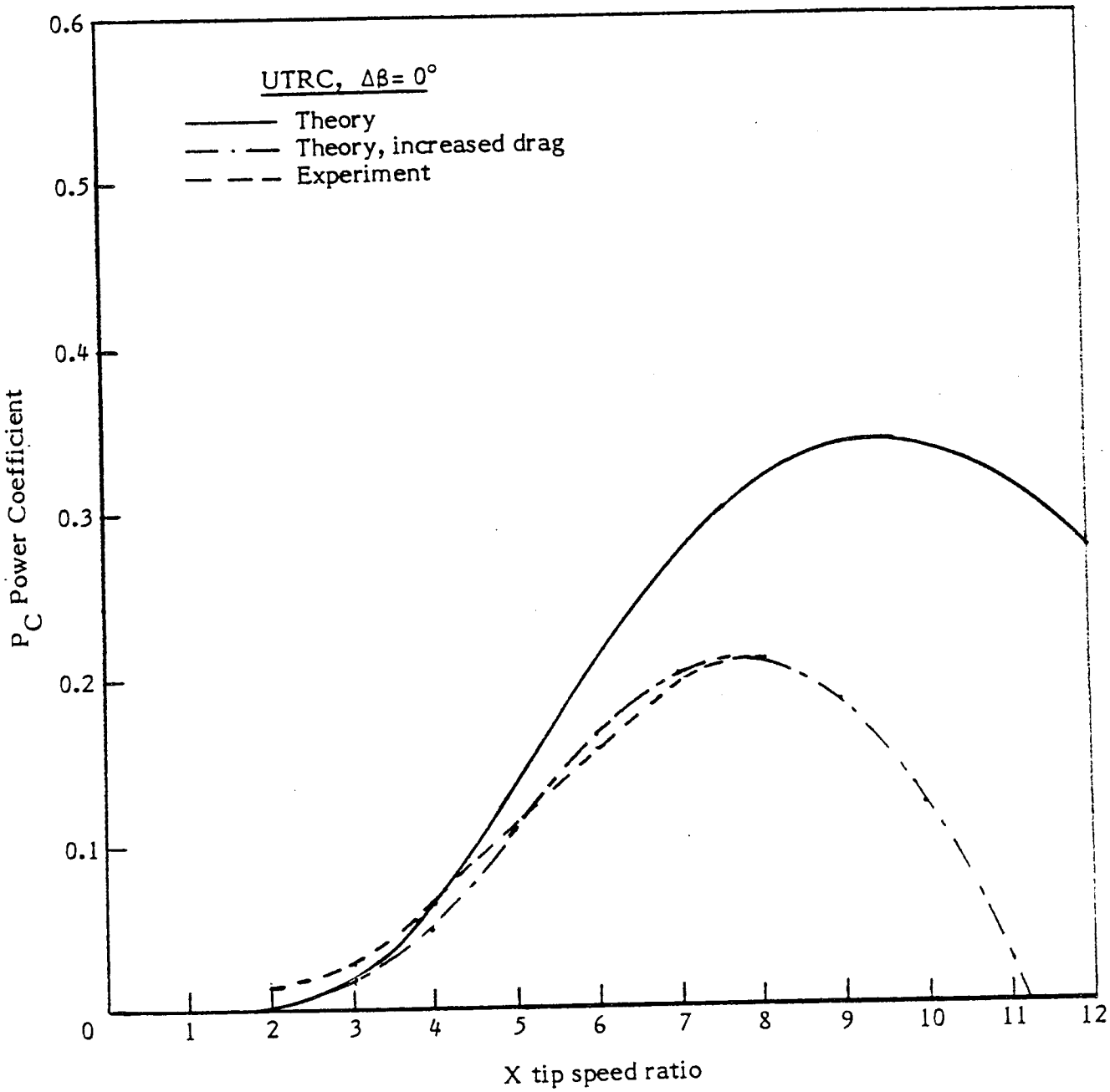

FIGURE 19. UTRC turbine comparison with theory, modified stalled flat-plate model.

7.0 RESULTS, CONCLUSIONS, AND RECOMMENDATIONS

7.1 Results

Examining the results of the analyses of the two rotors (data presented in Appendix A), a number of interesting conclusions can be drawn. Rotor A has a maximum P_C of 0.397 at design feather angle and a tip speed ratio of 5 to 5.5. However, at a feather angle of 4°, the maximum power coefficient is 0.442 at tip speed ratio of 6. Examination of the power coefficient curves reveals that performance is better at almost all tip speed ratios at this feather angle.

Rotor B has a maximum P_C of 0.337 at design feather angle and tip speed ratios of 8 to 8.5. Off design feather angles result in lower performance.

For both rotors it would appear that adding wind shear makes almost no difference in the performance. In fact, test cases have shown that even rotors as near to the ground as a MOD-2 rotor have only a three percent performance loss due to wind shear. The rotors under consideration have hub heights so great (normalized to rotor radius) that the wind speed variation is very small, resulting in the nearly insignificant performance change.

The effects due to choice of brake state model are more dramatic. At low tip speed ratios, there is no difference in the results as the rotor is not in the brake state. The changes in predicted performance occur at high advance ratios and/or negative feather angles. The advanced brake state model gives higher power coefficients at these points than the classical model. The curves given by the classical model tend to have an abrupt performance drop when the rotor enters the brake state. The advanced model tends to give smoother curves. Because the advanced model is based on observed data, it is felt that it will give performance predictions closer to the experimental results.

Comparison with experiment indicates that there is reasonable agreement with theory for Rotor A, the Enertech 1500, but poor agreement for Rotor B, the one-third-scale UTRC, for which the data was below the predicted curve. An increase in airfoil profile drag could account for the performance difference on the UTRC. (It is noted that Rockwell personnel indicated that this rotor had lower performance than expected.)

The computer model has been improved by changing the treatment of the stalled airfoil characteristics. A stalled flat plate model is used for the deep stall region (angle of attack greater than 26.5°) and an empirical shallow stall model has been used for angles between initial stall and 26.5°. Below initial stall, published airfoil data is used. This model has been called the modified-stalled-flat-plate model. These changes do provide a rational, theoretical basis for the stalled airfoil characteristics.

7.2 Conclusions

1. The PROP code in final form with proper airfoil characteristics can be used to calculate rotor performance over a broad range of blade geometries and tip speed ratio.

2. While the model has not been correlated with experiment for wind shear and brake state, primarily because of lack of data, the model has been shown to

give excellent agreement with data for the nominal design case of no-shear and no-brake state.

3. We conclude that the model is ready to be used as a design tool but requires that the user have a good working knowledge of airfoil characteristics for use on the turbine at the design Reynolds number.

7.3 Recommendations

To further improve the accuracy and usefulness of this computer program, the following investigations are needed:

1. Comparison with rotors operating in wind shear. Experimental rotors should be run in wind shears large enough to cause major changes in performance. Wake surveys should be conducted to ascertain how the performance varies about the circumference of the turbine.

2. Brake state model. Experiments are recommended to ascertain the accuracy of the brake state model currently used.

3. Off-axis flow. It is recommended that an experiment be conducted to determine how rotor performance varies in off-axis flow.

4. Airfoil characteristics. More information is needed on airfoil characteristics in the shallow stall regime. Further, it should be determined if these characteristics change in the rotating environment of a turbine blade due to centrifugal or other effects.

8.0 REFERENCES

1. Wilson, R.E. and P.B.S. Lissaman (1974): Applied aerodynamics of wind power machines. Oregon State University, Research Applied to National Needs (RANN), Under Grant No. GI-41840, May.

2. de Vries, O. (1979): Fluid dynamic aspects of wind energy conversion. AGARD-AG-243.

3. Wilson, R.E., P.B.S. Lissaman, and S.N. Walker (1976): Aerodynamic performance of wind turbines. Oregon State University, Research Applied to National Needs (RANN), under Grant No. AER 74-04014 A03, June.

4. Durand, W.F. (editor) (1934): Aerodynamic Theory, California Institute of Technology, Guggenheim Fund Publication.

5. Wentz, W.H., Jr., and J.T. Calhoun (1981): Analytical studies of new airfoils for wind turbines. Wind Turbine Dynamics, NASA Conference Publication 2185.

6. Sachs, P. (1974): Wind Forces in Engineering. Pergamon Press.

7. Davenport, A.G. (1961): The application of statistical concepts to the wind loading of structures. Proc. Institute of Civil Engineers, Vol. 19.

8. Horner, S.F. (editor) (1965): Fluid Mechanics Drag.

9. Critzos, C.C., H.H. Heyson, and R.W. Boswinkle, Jr. (1955): Aerodynamic characteristics of NACA 0012 airfoil section at angles of attack from 0^{o} to 180^{o}. National Advisory Committee for Aeronautics, Technical Note 3361.